*J. Fluid Mech.* (2021), *vol*. 916, A4, doi:10.1017/jfm.2021.199

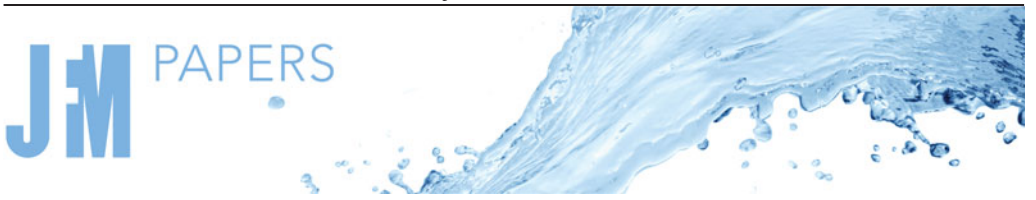

# Energy budget in decaying compressible MHD turbulence

**Yan Yang[1,2,3], Minping Wan[1,2,4,†], William H. Matthaeus[5] and Shiyi Chen[1,2,4]**

[1]Guangdong Provincial Key Laboratory of Turbulence Research and Applications, Southern University of Science and Technology, Shenzhen 518055, PR China

[2]Department of Mechanics and Aerospace Engineering, Southern University of Science and Technology, Shenzhen 518055, PR China

[3]University of Science and Technology of China, Hefei 230026, PR China

[4]Southern Marine Science and Engineering Guangdong Laboratory (Guangzhou), Guangzhou 511458, PR China

[5]University of Delaware, Newark, DE 19716, USA

(Received 21 September 2020; revised 2 February 2021; accepted 2 March 2021)

We study the decay of compressible magnetohydrodynamic (MHD) turbulence, emphasizing exchanges of energy between compressive and incompressive kinetic energies, magnetic energy, and thermal energy. A recently developed high order finite difference code is employed for compressible runs with a Mach number up to 2. Varying the nature of the initial conditions (magnitudes of velocity and magnetic fluctuations), and initial Mach numbers permits examination of various dynamical regimes characterized here by the changes between different energy reservoirs. Acoustic waves are responsible for the oscillatory exchange between compressive kinetic and thermal energy through the pressure dilatation term. The results indicate that exchange between kinetic and magnetic energy is dominated by interactions involving the solenoidal velocity. Several systematic rapid adjustments are found to be reproducible with simple scalings derived from the empirical data.

**Key words:** MHD turbulence, compressible turbulence, turbulence theory

## 1. Introduction

A basic feature of compressible magnetohydrodynamic (MHD) turbulence is the coexistence and interaction of several fields, that participate to varying degrees in different fundamental dynamic processes. For example, the compressive processes are related to acoustic waves, the shearing processes to vortical motions, the thermodynamic processes

† Email address for correspondence: wanmp@sustech.edu.cn

to the pressure, density and temperature, while the magnetic field will, in general, influence all other dynamics. These have inherently led to questions regarding the degree to which compressible MHD deviates from the incompressible case, and what role the magnetic field plays on the fluid motion, in contrast to purely hydrodynamic turbulence. The preponderance of work in turbulence has placed a great emphasis on either hydrodynamic turbulence or incompressible turbulence, with the advantages of simplification of the complicated physics underlying turbulence. However, compressible, magnetized turbulence plays an important role in many astrophysical processes (Elmegreen & Scalo 2004; Brandenburg & Lazarian 2013). Less has been accomplished in MHD turbulence research, and in particular, in research on compressible MHD turbulence, compared with research on incompressible hydrodynamic turbulence.

The first point that stands out in compressible MHD turbulence is the introduction of a magnetic field. In the usual way, the straightforward way to develop MHD turbulence theory is to generalize the formalism developed for hydrodynamic turbulence. For example, a standard MHD turbulence scenario inherited from hydrodynamics considers an energy cascade process over the inertial range. By applying considerations to MHD turbulence, in analogy with Kolmogorov's phenomenological theory, a third-order law in terms of Elsasser field increments has been proposed (Politano & Pouquet 1998; Carbone *et al.* 2009; Podesta 2008; Banerjee & Galtier 2013; Andrés *et al.* 2018; Hellinger *et al.* 2018). However, caution is required in doing this, since MHD flows differ from neutral fluids in many ways. There is a growing evidence – theoretical, observational and numerical – that universality might break down in MHD (Pouquet *et al.* 2010), including aspects of the energy spectrum (Kolmogorov 1941; Iroshnikov 1964; Kraichnan 1965) and of the local and nonlocal energy transfers (Aluie & Eyink 2010; Mininni 2011; Yang *et al.* 2016*a*; Grete *et al.* 2017) in MHD. At the same time, there are several processes in MHD turbulence that have no hydrodynamic counterpart, such as magnetic reconnection (Parker 1957), magnetic dynamo (Moffatt 1978) and several distinctive relaxation processes (Taylor 1974; Montgomery, Turner & Vahala 1978), to name a few. Therefore, intensive studies are necessary to understand new features specific to MHD turbulence.

The second point that stands out in compressible MHD turbulence is, of course, the effect of compressibility. In most treatises on turbulence theory, turbulence is assumed incompressible. For example, a $k^{-5/3}$ spectrum of density fluctuations has been reported in solar wind observations (Goldstein & Siscoe 1972) and interstellar remote sensing studies (Armstrong, Cordes & Rickett 1981), which was explained that density should act in part passively, supporting a pressure that, in effect, imposed a constraint (Montgomery, Brown & Matthaeus 1987; Shebalin & Montgomery 1988). This is suggestive that turbulence in the solar wind dominated by incompressible fluctuations, but compressibility remains an essential characteristic, both of interplanetary and interstellar plasmas (Spangler & Spitler 2004; Hnat, Chapman & Rowlands 2005; Federrath *et al.* 2010; Chen *et al.* 2012; Banerjee *et al.* 2016*a*; Chen 2016; Roberts *et al.* 2017; Shoda *et al.* 2019). Evidently one must appeal to a compressible MHD model. Compressible MHD turbulence, in the presence of waves or shocks, is expected to admit features beyond what has been seen in the incompressible case, such as the energy cascade process incorporating compressibility effects (Banerjee *et al.* 2016*b*; Hadid, Sahraoui & Galtier 2017; Hadid *et al.* 2018; Andrés *et al.* 2019). In the nonlinear regime, different scaling relations emerge (Lithwick & Goldreich 2001; Beresnyak, Lazarian & Cho 2005; Kowal & Lazarian 2007; Benzi *et al.* 2008; Schmidt, Federrath & Klessen 2008; Lemaster & Stone 2009; Kritsuk, Wagner & Norman 2013; Wang, Gotoh & Watanabe 2017; Yang *et al.* 2017) due to the influence of shocks. The shock is usually identified by a very rapid increase in the field (cliff) followed by a more

gradual or smooth decrease (ramp), ramp-cliff structure for scalar turbulence (Sreenivasan 1991; Celani *et al.* 2000, 2001). Carbone *et al.* (2018) applied the arbitrary-order Hilbert spectral analysis (Huang *et al.* 2010), to extract scaling information for solar wind proton density fluctuations measured by the BMSW instrument on the *Spektr-R* spacecraft. By minimizing the effect of the ramp–cliff structures, the resulting scaling exponents in the inertial range were close to those for velocity fluctuations obtained through the structure functions in hydrodynamic turbulence. Another related aspect which could arise from shocks is the $k^{-2}$ (Roberts & Goldstein 1987; Burlaga, Mish & Roberts 1989; Bec & Khanin 2007; Wang *et al.* 2013; Bruno *et al.* 2014; Yang *et al.* 2016*a*) or shallower than $k^{-2}$ (Siscoe *et al.* 1968; Borovsky 2010) spectrum. The compressibility can be controlled by virtue of varying kinetic energy injection (Kida & Orszag 1990; Federrath *et al.* 2010; Yang *et al.* 2016*a*; Cerretani & Dmitruk 2019), e.g. from divergence-free to curl-free, which plays an important role in amplification of the magnetic field (Federrath *et al.* 2011).

The pioneering work by Klainerman & Majda (1981, 1982) has provided a firm mathematical basis for understanding how, in specific circumstances, solutions to compressible flow equations approach, at low Mach numbers, solutions to incompressible flow equations. This is extended to spatially homogeneous MHD in a formalism usually called 'nearly incompressible' (NI) theory (Matthaeus & Brown 1988; Zank & Matthaeus 1990, 1993) and subsequently to inhomogeneous MHD (Bhattacharjee, Ng & Spangler 1998; Bhattacharjee *et al.* 1999; Hunana & Zank 2010). One immediate consequence arising from NI theory is the close similarity in physics of compressible and incompressible systems, such as the dominance of vorticity. In these formalisms, the solution to compressible flow equations is expanded in powers of Mach number ($M_t$). In the NI regime, the density variation is of order $O(M_t^2)$, and the ratio of compressible velocity fluctuations $u_L$ to incompressible velocity fluctuations $u_T$ is of order $O(M_t)$. (Note that the requirement that $u_L/u_T = O(M_t)$ is the formal condition found for NI behaviour in hydrodynamics (Klainerman & Majda 1981) and in high beta MHD (Matthaeus & Brown 1988). However the more restrictive scaling $u_L/u_T = O(M_t^2)$ has also been examined in some numerical studies (Ghosh & Matthaeus 1992; Cerretani & Dmitruk 2019).) As the strength of acoustic waves becomes comparable to the vortical motions, i.e. the ratio of compressible to incompressible velocity fluctuations is of order $O(1)$, the nearly incompressible asymptotic expansion breaks down and the flow enters a modally equipartitioned compressible (MEC) state. This situation has been addresses by Kraichnan (1955) which permits strong waves and the density variation is of order $O(M_t)$. Another possibility was less considered to date is the compressible wave (CW) state, i.e. pure acoustic waves. One physically plausible feature in this model is the dominance of acoustic waves over vortical motions, as suggested by Ghosh & Matthaeus (1992) and Cerretani & Dmitruk (2019), but there is no theoretical basis on the scaling for velocity fluctuations nor for density variations.

The richness of results in compressible MHD turbulence, there being some apparently conflicting tendencies, adds considerably to the motivation for finding systematically repeatable behaviours. A decomposition of the turbulent field is frequently implemented to study different compressible MHD turbulence processes. For example, characteristics for three separate propagating linear eigenmodes – the Alfvén mode, the slow magnetosonic mode and the fast magnetosonic mode have been studied using numerical simulations (Cho & Lazarian 2002; Kowal & Lazarian 2010; Yang *et al.* 2018; Makwana & Yan 2020) and observations (Yao *et al.* 2011; Howes *et al.* 2012; Klein *et al.* 2012). In this work, we decompose the velocity field into solenoidal and compressive parts following Helmholtz decomposition as used in Kida & Orszag (1990, 1992), Miura & Kida (1995), Pan & Johnsen (2017), Wang *et al.* (2019). The decay of energy in a turbulent MHD system is both

an interesting academic problem and also an important practical one. A number of studies have been devoted to trying to understand aspects of this process, such as the energy decay law (Hossain *et al.* 1995; Kinney, McWilliams & Tajima 1995; Galtier, Politano & Pouquet 1997; Mac Low *et al.* 1998; Stone, Ostriker & Gammie 1998; Mac Low 1999; Padoan & Nordlund 1999; Biskamp & Müller 1999; Bigot, Galtier & Politano 2008; Brandenburg & Kahniashvili 2017), the selective decay and dynamic alignment relaxation theories (Taylor 1974; Montgomery *et al.* 1978; Stribling & Matthaeus 1991; Ghosh & Matthaeus 1990), and the similarity decay (Wan *et al.* 2012; Bandyopadhyay *et al.* 2019). To get a further insight into the decaying MHD system, here we inquire how different types of energy (including solenoidal kinetic, compressive kinetic, magnetic and thermal energies) interact, which was also investigated in turbulent magnetohydrodynamic jets recently in Praturi & Girimaji (2020) and in the evolution of the Kelvin–Helmholtz instability in Salvesen *et al.* (2014). Similar analysis in compressible hydrodynamic turbulence can be found in Kida & Orszag (1990, 1992), Miura & Kida (1995) and Pan & Johnsen (2017).

In this paper, we commence with the simplest case, having no external imposed magnetic field, no forcing, unit magnetic Prandtl number and vanishing cross helicity, and report results from a series of numerical simulations. We study the energy budget in decaying compressible MHD turbulence, paying particular attention to the interaction and exchange between the differing components and its dependence on initial configurations. The equations and the definition of the decomposed energies are given in § 2. Details of the simulations are given in § 3. The exchange between solenoidal kinetic, compressive kinetic, magnetic and thermal energy are discussed in §§ 4 and 5. In § 6, we present three short-time energy amplification processes, and in § 7 a brief discussion of the behaviour of plasma $\beta$. Conclusions and discussion of the results are given in § 8.

## 2. Formulation

### 2.1. *MHD equations*

Compressible MHD equations are

$$\partial_t \rho + \boldsymbol{\nabla} \cdot (\rho \boldsymbol{u}) = 0, \tag{2.1}$$

$$\partial_t (\rho \boldsymbol{u}) + \boldsymbol{\nabla} \cdot \left[ \rho \boldsymbol{u}\boldsymbol{u} + p\boldsymbol{I} + \tfrac{1}{2}\left(\boldsymbol{b}^2\right)\boldsymbol{I} - \boldsymbol{b}\boldsymbol{b} \right] = \boldsymbol{\nabla} \cdot \boldsymbol{\sigma}, \tag{2.2}$$

$$\partial_t \boldsymbol{b} + \boldsymbol{\nabla} \cdot (\boldsymbol{u}\boldsymbol{b} - \boldsymbol{b}\boldsymbol{u}) = \eta \nabla^2 \boldsymbol{b}, \tag{2.3}$$

$$\begin{aligned} \partial_t \mathcal{E} + \boldsymbol{\nabla} \cdot \left[ \left( \mathcal{E} + p + \tfrac{1}{2}\boldsymbol{b}^2 \right) \boldsymbol{u} - (\boldsymbol{b}\boldsymbol{b}) \cdot \boldsymbol{u} \right] \\ = \boldsymbol{\nabla} \cdot (\kappa \boldsymbol{\nabla} T) + \boldsymbol{\nabla} \cdot (\boldsymbol{\sigma} \cdot \boldsymbol{u}) + \boldsymbol{\nabla} \cdot [\boldsymbol{b} \times (\eta \boldsymbol{\nabla} \times \boldsymbol{b})], \end{aligned} \tag{2.4}$$

where $\rho$, $\boldsymbol{u}$, $p$, $T$, $\boldsymbol{b}$ and $\mathcal{E} = \rho \boldsymbol{u} \cdot \boldsymbol{u}/2 + p/(\gamma - 1) + \boldsymbol{b} \cdot \boldsymbol{b}/2 = E_k + E_{th} + E_b$ denote density, velocity, pressure, temperature, magnetic field and total (kinetic, thermal and magnetic) energy. $\gamma$ is the adiabatic index with a value, $\gamma = 1.4$; $\boldsymbol{I}$ is the unity tensor; $\sigma_{ij} = \mu(\partial_i u_j + \partial_j u_i) - 2(\mu(\boldsymbol{\nabla} \cdot \boldsymbol{u})\delta_{ij})/3$ is the viscous stress tensor; $\mu$ is the dynamic viscosity; $\eta$ is the magnetic diffusivity; and $\kappa$ is the thermal conductivity. The MHD equations are closed with the equation of state of an ideal gas. This set of compressible MHD equations is expected to be valid in a conducting ideal gas such as a hydrogen plasma when collisions are dominant and the medium is isotropic so that the dissipation coefficients are scalars.

The MHD equations are non-dimensionalized by introducing several reference scales. For example, length is normalized to $L_0$, velocity to $U_0$, density to $\rho_0$, magnetic field to $B_0$, temperature to $T_0$, viscosity to $\mu_0$, magnetic diffusivity to $\eta_0$ and thermal conductivity to $\kappa_0$. Then the system is control by several dimensionless parameters, such as the Reynolds number $Re = \rho_0 U_0 L_0/\mu_0$, the magnetic Reynolds number $Re_m = U_0 L_0/\eta_0$ and the Mach number $M = U_0/c_{s,0}$, where $c_{s,0} = \sqrt{\gamma R T_0}$ is the reference sound speed and $R$ is the universal gas constant. The dimensionless $\mu$, $\kappa$ and $\eta$ (here we use the same symbols as dimensional ones without confusion) are assumed to be described by the Sutherland's law as used by Yang *et al.* (2016*b*), $\mu = \kappa = \eta = 1.4042T^{3/2}/(T + 0.4042)$.

### 2.2. *Helmholtz decomposition*

To clarify the interchange among differing components, the Helmholtz decomposition is employed (as used in Kida & Orszag 1992; Miura & Kida 1995; Pan & Johnsen 2017) to separate compressible and incompressible motions of the velocity field. It can be applied to the Fourier transform $\hat{\boldsymbol{v}}(\boldsymbol{k})$ of any vector field $\boldsymbol{v}(\boldsymbol{x})$ of zero mean, which decomposes $\hat{\boldsymbol{v}}$ into components along and normal to $\boldsymbol{k}$

$$\hat{\boldsymbol{v}} = \hat{\boldsymbol{v}}_c + \hat{\boldsymbol{v}}_s, \tag{2.5}$$

where $\hat{\boldsymbol{v}}_c = \boldsymbol{k}(\boldsymbol{k}\cdot\hat{\boldsymbol{v}})/k^2$ is the compressive (longitudinal) part and $\hat{\boldsymbol{v}}_s = -(\boldsymbol{k}\times(\boldsymbol{k}\times\hat{\boldsymbol{v}})/k^2)$ is the solenoidal (transverse) part. After accomplishing this separation, it is straightforward to reassemble the velocity in real space (or Fourier-space) into incompressible and compressible parts. For flows that are potentially strongly compressive, it is convenient to gauge the relative amplitudes of these motions with a density weighting. We introduce a variable $\boldsymbol{w} = \sqrt{\rho}\boldsymbol{u}$. The r.m.s. value of the compressive part of $\boldsymbol{w}$ will be written as the longitudinal part $u_L$, while the r.m.s. value of the solenoidal part of $\boldsymbol{w}$ is designated as the transverse part $u_T$. In general this differs slightly from the decomposition of the velocity itself into transverse and longitudinal parts, as has been customary in the theory of nearly incompressible flows (Klainerman & Majda 1982; Matthaeus & Brown 1988; Ghosh & Matthaeus 1992). However in the limit of low Mach number and incompressibility the two approaches coincide. With these definitions, the kinetic energy can be decomposed into compressive and solenoidal parts as follows.

From (2.1) and (2.2), we have

$$\partial_t \boldsymbol{w} = \boldsymbol{A} + \boldsymbol{P} + \boldsymbol{M} + \boldsymbol{D}, \tag{2.6}$$

where

$$\boldsymbol{A} = -\left[(\boldsymbol{u}\cdot\nabla)\boldsymbol{w} + \tfrac{1}{2}\boldsymbol{w}\nabla\cdot\boldsymbol{u}\right], \tag{2.7}$$

$$\boldsymbol{P} = -\frac{\nabla p}{\sqrt{\rho}}, \tag{2.8}$$

$$\boldsymbol{M} = \frac{(\nabla\times\boldsymbol{b})\times\boldsymbol{b}}{\sqrt{\rho}} = -\frac{\nabla(\boldsymbol{b}^2/2)}{\sqrt{\rho}} + \frac{(\boldsymbol{b}\cdot\nabla)\boldsymbol{b}}{\sqrt{\rho}}, \tag{2.9}$$

$$\boldsymbol{D} = \frac{\nabla\cdot\boldsymbol{\sigma}}{\sqrt{\rho}}. \tag{2.10}$$

Note that the Lorentz force $\boldsymbol{M}$ is composed of magnetic pressure term, $\boldsymbol{M}_1 = -\nabla(\boldsymbol{b}^2/2)/\sqrt{\rho}$ and remaining stress term $\boldsymbol{M}_2 = (\boldsymbol{b}\cdot\nabla)\boldsymbol{b}/\sqrt{\rho}$. Accordingly, the evolution

of the decomposed kinetic energy spectra can be derived from (2.6) as

$$\partial_t E_{k,\alpha}(k,t) = A_\alpha(k,t) + P_\alpha(k,t) + M_\alpha(k,t) + D_\alpha(k,t), \tag{2.11}$$

where the subscript $\alpha = c, s$ represents compressive and solenoidal parts, respectively.

$$E_{k,\alpha}(k,t) = \sum_{k-0.5\leqslant|\boldsymbol{k}|<k+0.5} \tfrac{1}{2}\hat{\boldsymbol{w}}_\alpha(\boldsymbol{k},t)\cdot\hat{\boldsymbol{w}}^*_\alpha(\boldsymbol{k},t), \tag{2.12}$$

$$A_\alpha(k,t) = \sum_{k-0.5\leqslant|\boldsymbol{k}|<k+0.5} \hat{\boldsymbol{w}}^*_\alpha(\boldsymbol{k},t)\cdot\hat{\boldsymbol{A}}_\alpha(\boldsymbol{k},t), \tag{2.13}$$

$$P_\alpha(k,t) = \sum_{k-0.5\leqslant|\boldsymbol{k}|<k+0.5} \hat{\boldsymbol{w}}^*_\alpha(\boldsymbol{k},t)\cdot\hat{\boldsymbol{P}}_\alpha(\boldsymbol{k},t), \tag{2.14}$$

$$M_\alpha(k,t) = \sum_{k-0.5\leqslant|\boldsymbol{k}|<k+0.5} \hat{\boldsymbol{w}}^*_\alpha(\boldsymbol{k},t)\cdot\hat{\boldsymbol{M}}_\alpha(\boldsymbol{k},t), \tag{2.15}$$

$$D_\alpha(k,t) = \sum_{k-0.5\leqslant|\boldsymbol{k}|<k+0.5} \hat{\boldsymbol{w}}^*_\alpha(\boldsymbol{k},t)\cdot\hat{\boldsymbol{D}}_\alpha(\boldsymbol{k},t). \tag{2.16}$$

Summing (2.11) over all shells yields the evolution of spatially averaged kinetic energy, $\langle E_{k,\alpha}\rangle(t) = \sum_k E_{k,\alpha}(k,t)$, with spatial averages of the quantities in (2.12)–(2.16) analogously defined,

$$\partial_t\langle E_{k,\alpha}\rangle = \langle A_\alpha\rangle + \langle P_\alpha\rangle + \langle M_\alpha\rangle + \langle D_\alpha\rangle. \tag{2.17}$$

In this equation we identify the various terms as

(i) $\langle A_\alpha\rangle$ is the advection term that exchanges kinetic energy between compressive and solenoidal types. $\langle A_c\rangle + \langle A_s\rangle$=0 for periodic boundary condition.
(ii) $\langle P_\alpha\rangle$ is the pressure-dilatation term that exchange energy between type $\alpha$ kinetic and thermal components.
(iii) $\langle M_\alpha\rangle$ is the Lorentz force term that represents the exchange of type $\alpha$ kinetic and magnetic energy.
(iv) $\langle D_\alpha\rangle$ is the viscous dissipation term of kinetic energy of type $\alpha$.

In summary, we focus on four types of energy: solenoidal kinetic energy $\langle E_{k,s}\rangle$, compressive kinetic energy $\langle E_{k,c}\rangle$ (as defined in (2.17)), magnetic energy $\langle E_b\rangle = \langle \boldsymbol{b}\cdot\boldsymbol{b}/2\rangle$ and thermal energy $\langle E_{th}\rangle = \langle p/(\gamma-1)\rangle$, and the channels in (2.17) concerning their exchange.

## 3. Simulation details

We solve the compressible MHD equation via a hybrid scheme (Yang *et al.* 2016*b*; Yang 2019), which couples a sixth-order compact finite difference scheme for smooth regions and a fifth-order weighted essentially non-oscillatory (WENO) scheme for shock regions. The fields are advanced in time by a third-order Runge–Kutta method. All runs discussed here are freely decaying initial value problems conducted in periodic $(2\pi)^3$ geometry with $512^3$ grid points. The magnetic Prandtl number is $Pm = 1$, and we do not impose an external magnetic field. All runs have initially uniform density and temperature. The velocity and magnetic fields are initialized at Fourier modes $1 \leqslant |\boldsymbol{k}| \leqslant 8$ with random phases, and with modal spectra proportional to $1/[1 + (k/k_c)^{8/3}]$ with $k_c = 3$. The initial cross helicity, $H_c = 2\langle \boldsymbol{u}\cdot\boldsymbol{b}\rangle/\langle \boldsymbol{u}^2 + \boldsymbol{b}^2\rangle$, though not exactly zero, is very small.

To study the energy transfer among solenoidal kinetic $\langle E_{k,s}\rangle$, compressive kinetic $\langle E_{k,c}\rangle$, magnetic $\langle E_b\rangle$ and thermal energy $\langle E_{th}\rangle$, we initialize our system with a range of Mach numbers and a variety of initial velocity and magnetic fluctuations. These runs are grouped into four series that respectively emphasize time variations of these four types of energy. We briefly summarize these runs in the following, and more details are listed for each run in table 1. Note that the Taylor-scale Reynolds number $Re_\lambda$, which is always used to compare the turbulence between different flows, is defined as

$$Re_\lambda = Re\frac{u_{rms}\lambda\rho}{\mu}, \tag{3.1}$$

where $u_{rms} = \sqrt{\langle \boldsymbol{u}\cdot\boldsymbol{u}\rangle/3}$ is the r.m.s velocity, $\lambda = u_{rms}/\omega_{rms}$ is the Taylor microscale and $\omega_{rms}$ is the r.m.s. value of vorticity $\boldsymbol{\omega} = \boldsymbol{\nabla}\times\boldsymbol{u}$. The turbulent Mach number $M_t$, related to compressibility in some sense, is defined as

$$M_t = M\frac{\sqrt{\langle \boldsymbol{u}\cdot\boldsymbol{u}\rangle}}{\sqrt{T}}, \tag{3.2}$$

where $T$ is the temperature. Varying velocity field could result in different $Re_\lambda$ and $M_t$ as listed in table 1. The large-eddy turnover times for the runs are different and vary with time (initial large-eddy turnover time $\sim$2.0), so the time throughout the paper will be in code units.

The first series of runs, listed as Type T in table 1, emphasizes energy interchange between compressive kinetic energy and thermal components, here commencing with equal amplitude of compressive velocity field energy and magnetic energy, $\langle E_{k,c}\rangle_0 = \langle E_b\rangle_0 = 0.5$ and an absence of a solenoidal kinetic energy component. Three values of initial turbulent Mach number $M_t = 0.1, 0.5, 1.0$ are used.

The second series of runs, Type S, are similar to the first series of type T runs in that only the compressive kinetic and magnetic components are excited, but with varying amplitudes ranging from 0.0 to 0.5. These runs are intended to clarify which energy reservoir is the main contributor to supplying solenoidal kinetic energy.

The third series of runs have varying turbulent Mach numbers and amplitudes of solenoidal kinetic and magnetic energy. This series of runs is devised to study the growth of compressive kinetic energy and its dependence on Mach number, which are referred to as type C.

Runs in the fourth series are initialized with a mixture of solenoidal and compressive kinetic components. Note that the compressible MHD with quite a small initial magnetic energy behaves like compressible hydrodynamics, e.g. S09 and C04, since the magnetic energy tends to dissipate out of the system rapidly, without substantially interacting with the kinetic part. Therefore, a small amount of magnetic energy is introduced in the beginning to avoid reducing immediately to hydrodynamic-like dynamics and, at the same time, to address questions concerning magnetic field amplification (dynamo). We refer to this set of runs as type B.

To quantify the contribution from solenoidal kinetic energy to magnetic energy, we make a specific comparison to type B runs by introducing a series of incompressible runs labelled as type I. We numerically solve the incompressible MHD equations (see appendix A) in periodic $(2\pi)^3$ geometry using the standard pseudo-spectral method with de-aliasing by the two-thirds rule. The fields are advanced in time by a second-order Adam–Bashforth scheme. All other parameters are set up in the same way as the compressible runs. In table 1 we show the initial kinetic energy at changing its amplitude from 0.15 to 0.5. We do not conduct a corresponding incompressible run to B05 since its initial state is nearly uniform and still.

| Run | $N^3$ | $M_t$ | $Re_\lambda$ | $\langle E_{k,s}\rangle_0$ | $\langle E_{k,c}\rangle_0$ | $\langle E_b\rangle_0$ |
|---|---|---|---|---|---|---|
| T01 | $512^3$ | 0.1 | 356 | 0.00 | 0.50 | 0.50 |
| T02 | $512^3$ | 0.5 | 356 | 0.00 | 0.50 | 0.50 |
| T03 | $512^3$ | 1.0 | 356 | 0.00 | 0.50 | 0.50 |
| S01 | $512^3$ | 0.0 | 0.0 | 0.00 | 0.00 | 0.50 |
| S02 | $512^3$ | 0.55 | 195 | 0.00 | 0.15 | 0.50 |
| S03 | $512^3$ | 0.71 | 252 | 0.00 | 0.25 | 0.50 |
| S04 | $512^3$ | 0.84 | 298 | 0.00 | 0.35 | 0.50 |
| S05 | $512^3$ | 1.0 | 356 | 0.00 | 0.50 | 0.50 |
| S06 | $512^3$ | 1.0 | 356 | 0.00 | 0.50 | 0.35 |
| S07 | $512^3$ | 1.0 | 356 | 0.00 | 0.50 | 0.25 |
| S08 | $512^3$ | 1.0 | 267 | 0.00 | 0.50 | 0.15 |
| S09 | $512^3$ | 1.0 | 267 | 0.00 | 0.50 | $1.00 \times 10^{-4}$ |
| C01 | $512^3$ | 0.1 | 623 | 0.50 | 0.00 | 0.50 |
| C02 | $512^3$ | 1.0 | 623 | 0.50 | 0.00 | 0.50 |
| C03 | $512^3$ | 2.0 | 623 | 0.50 | 0.00 | 0.50 |
| C04 | $512^3$ | 1.0 | 623 | 0.50 | 0.00 | $1.00 \times 10^{-4}$ |
| B01 | $512^3$ | 1.0 | 623 | 0.50 | 0.00 | 0.025 |
| B02 | $512^3$ | 1.0 | 491 | 0.35 | 0.15 | 0.025 |
| B03 | $512^3$ | 1.0 | 438 | 0.25 | 0.25 | 0.025 |
| B04 | $512^3$ | 1.0 | 399 | 0.15 | 0.35 | 0.025 |
| B05 | $512^3$ | 1.0 | 213 | 0.00 | 0.50 | 0.025 |
| I01 | $512^3$ | — | 611 | 0.50 | — | 0.025 |
| I02 | $512^3$ | — | 511 | 0.35 | — | 0.025 |
| I03 | $512^3$ | — | 432 | 0.25 | — | 0.025 |
| I04 | $512^3$ | — | 335 | 0.15 | — | 0.025 |

Table 1. Simulation parameters: grid size $N^3$, initial turbulent Mach number $M_t = M(\sqrt{\langle \boldsymbol{u}\cdot\boldsymbol{u}\rangle}/\sqrt{T})$ where $T$ is the temperature, initial Taylor-scale Reynolds number $Re_\lambda = Re(u_{rms}\lambda\rho/\mu)$ where $u_{rms}$ is the r.m.s. velocity and $\lambda$ is the Taylor microscale, initial solenoidal kinetic, compressive kinetic and magnetic energy $\langle E_{k,s}\rangle_0$, $\langle E_{k,c}\rangle_0$, $\langle E_b\rangle_0$. Note that T03 and S05 runs are the same.

## 4. Acoustic energy exchange

Here, we consider the energy exchange between compressive kinetic and thermal components. Based on (2.17), it is clear that the pressure dilatation and the viscous dissipation are two alternatives that can couple kinetic and thermal energy. But unlike the viscous dissipation, the point-wise pressure dilatation is not positive definite. We expect that the pressure dilatation exchanges energy between solenoidal kinetic and thermal forms at a significantly diminished level, since this term arises mainly from compressibility effects. Therefore, we focus on type T runs in this section, which are initialized with purely compressible motion to generate as strongly compressed flows as possible.

We proceed with the T01 run at low initial turbulent Mach number $M_t = 0.1$. The time histories of solenoidal kinetic, compressive kinetic, magnetic and thermal energy are shown in figure 1. The total (kinetic, thermal and magnetic) energy is conserved. The thermal energy $\langle E_{th}\rangle$ keeps increasing on average partially due to the energy supply from kinetic and magnetic energy through viscous and resistive dissipation. Also noteworthy, is the regular oscillation in compressive kinetic and thermal energy, while solenoidal kinetic and magnetic energy varies with time smoothly. It is widely recognized that compressive velocity field is inherently wave-like and thus associated with oscillatory characters.

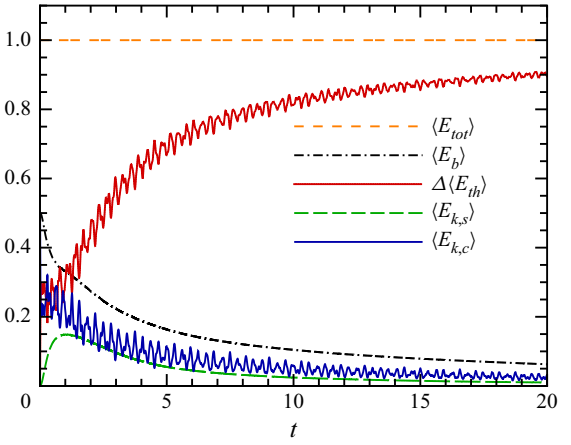


Figure 1. Time histories of solenoidal kinetic $\langle E_{k,s}\rangle$, compressive kinetic $\langle E_{k,c}\rangle$, magnetic $\langle E_b\rangle$ and thermal energy $\langle E_{th}\rangle$ for T01 run. The change in thermal energy from its initial value $\Delta\langle E_{th}\rangle$ is plotted. The total energy (sum of the four energies in the plot) $\langle E_{tot}\rangle$ is conserved.

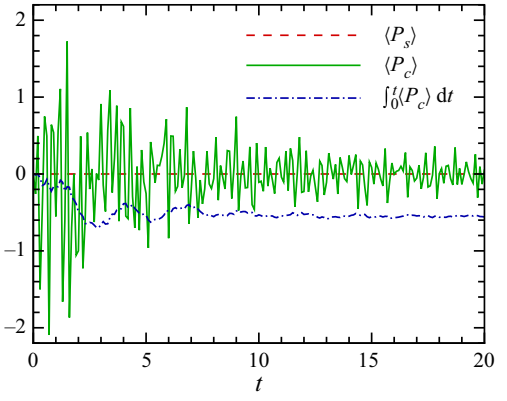


Figure 2. Time evolutions of solenoidal $\langle P_s\rangle$ and compressive parts $\langle P_c\rangle$ of pressure dilatation and its time integral for T01 run.

Similar oscillations have been reported in compressible hydrodynamic turbulence (Kida & Orszag 1992; Sarkar 1992; Miura & Kida 1995; Ristorcelli 1997; Lee, Yu & Girimaji 2006; Pan & Johnsen 2017; Praturi & Girimaji 2019), which is attributed to the pressure-dilatation term $\langle P_c\rangle$. It is natural to expect that this reasoning is still applicable to our cases, even though both pressure and dilatation might be affected by the magnetic field. One may recall that the interference of linear Alfvén waves could lead to oscillatory exchanges between kinetic and magnetic energies (Pouquet, Sulem & Meneguzzi 1988). The Alfvén speed is much smaller than the sound speed here, thus merely introducing minor effects on the wavelike character. We show the time history of pressure dilatation in figure 2. The solenoidal part of pressure dilatation $\langle P_s\rangle$ is negligible, while the compressive part $\langle P_c\rangle$ evidently exhibits oscillations. Although the time history of the pressure dilatation is not sign-definite, as energy may be transferred into or out of thermal energy, its time integral indicates net transfer into thermal energy.

The results at higher Mach number are shown in figure 3, where one can see slight evolutionary differences in magnetic and solenoidal kinetic energy, while compressive kinetic and thermal energy oscillate with distinct periods. A higher Mach number leads

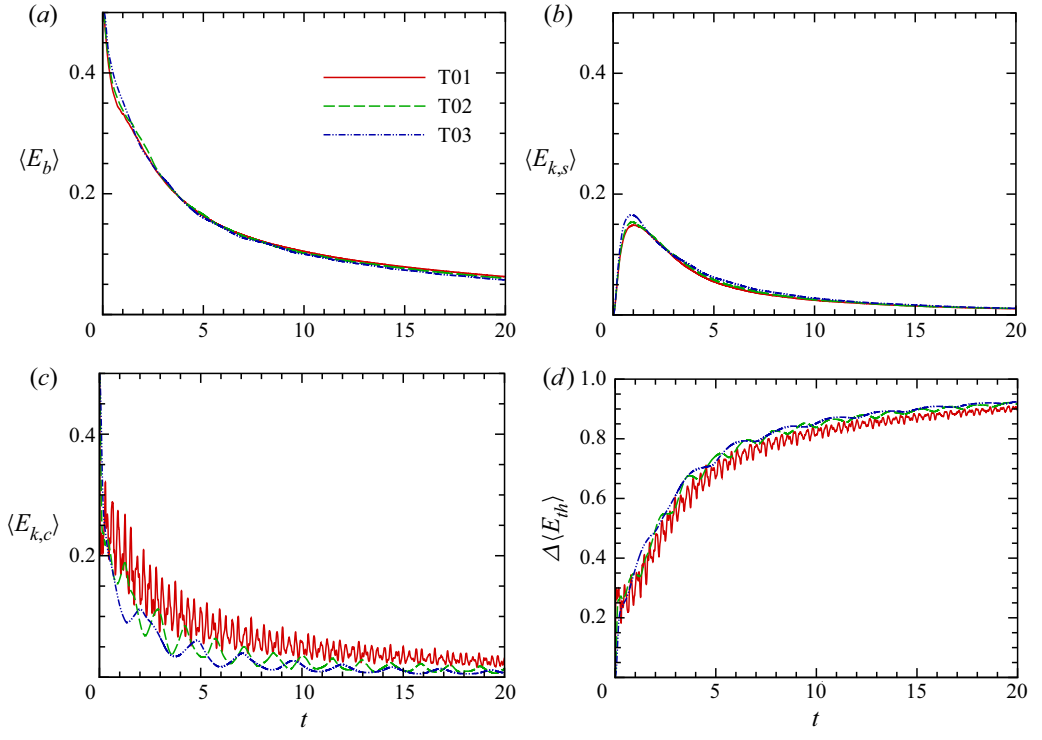


Figure 3. Time histories of magnetic $\langle E_b \rangle$, solenoidal kinetic $\langle E_{k,s} \rangle$, compressive kinetic $\langle E_{k,c} \rangle$ and thermal energy $\langle E_{th} \rangle$ in type T runs with initial turbulent Mach number $M_t = 0.1, 0.5, 1.0$. The change in thermal energy from its initial value $\Delta\langle E_{th} \rangle$ is plotted.

| Run | $M_t$ | $c_s$ | $\tau$ | $\tau_{linear}$ |
|---|---|---|---|---|
| T01 | 0.1 | 10.0 | 0.3 | 0.3 |
| T02 | 0.5 | 2.1 | 1.4 | 1.5 |
| T03 | 1.0 | 1.2 | 2.5 | 2.6 |

Table 2. Initial turbulent Mach number $M_t$, time averaged sound speed $c_s$,[a] period of oscillations $\tau$ and period of oscillations estimated from linear theory $\tau_{linear} = \pi/c_s$.

[a]The sound speed increases slightly with time in these simulations.

to longer periods of the oscillation; this is quantitatively listed in table 2. Also listed is an estimated period from linear theory $\tau_{linear} = \pi/c_s$ ($c_s$ is the sound speed), which agrees well with the period from the simulation $\tau$. This suggests that acoustic waves take part in the compressible kinetic-thermal energy exchange channel. The procedure for estimating the period is detailed in the following.

We consider the simplest case of homogeneous compressible MHD described by $\rho_0$, $p_0$, $\boldsymbol{u}_0$ and $\boldsymbol{b}_0$. The initial uniform state is $\rho_0 = 1$, $\boldsymbol{u}_0 = 0$ and $\boldsymbol{b}_0 = 0$. For sufficiently small perturbations, $\rho'$, $p'$, $\boldsymbol{u}'$ and $\boldsymbol{b}'$, we can linearize the MHD equations (2.2) and (2.4) as

$$\partial_t \boldsymbol{u}' = -\boldsymbol{\nabla} p', \tag{4.1}$$

$$\partial_t p' = -\gamma p_0 \boldsymbol{\nabla} \cdot \boldsymbol{u}', \tag{4.2}$$

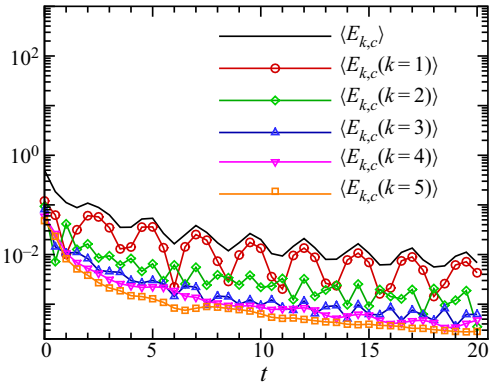


Figure 4. Time history of compressive kinetic energy at different wavenumbers for T03 run.

neglecting diffusive processes for simplicity. These equations can be reduced to a single one for $p'$:

$$\frac{\partial^2 p'}{\partial t^2} = c_s^2 \nabla^2 p', \tag{4.3}$$

which can be written in Fourier space as

$$\frac{\partial^2 \widehat{p'}(\boldsymbol{k}, t)}{\partial t^2} = -c_s^2 k^2 \widehat{p'}(\boldsymbol{k}, t). \tag{4.4}$$

The solution to this wave equation is a combination of wave functions,

$$\widehat{p'}(\boldsymbol{k}, t) = A\, \mathrm{e}^{-\mathrm{i}c_s k t} + B\, \mathrm{e}^{\mathrm{i}c_s k t}, \tag{4.5}$$

where complex numbers $A, B$ depend on initial and boundary conditions. Velocity fluctuation $\boldsymbol{u}'$ is obtained by substituting (4.5) for $p'$ in (4.1). Then the pressure dilatation term is

$$P(k, t) = \sum_{1-0.5 \leqslant |\boldsymbol{k}| < 1+0.5} \frac{2k}{c_s} \mathrm{Im}(A^* B\, \mathrm{e}^{2\mathrm{i}c_s k t}). \tag{4.6}$$

A similar expression has been obtained by Miura & Kida (1995).

The period of oscillation is different at different wave numbers, but that of compressive kinetic energy is determined by the smallest wavenumber ($k = 1$), which is the dominant mode in our cases, as shown in figure 4. At the smallest wavenumber ($k = 1$),

$$P(k = 1, t) = \sum_{1-0.5 \leqslant |\boldsymbol{k}| < 1+0.5} \frac{2}{c_s} \mathrm{Im}(A^* B\, \mathrm{e}^{2\mathrm{i}c_s t}). \tag{4.7}$$

The period of oscillation estimated from the linear theory is $\tau_{linear} = \pi / c_s$.

## 5. Energy transfer among kinetic and magnetic components

We consider the energy interchange among solenoidal kinetic, compressive kinetic and magnetic components through the advection term $\langle A_\alpha \rangle$ and the Lorentz force term $\langle M_\alpha \rangle$, where again, $\alpha = c$ or $s$ indicates compressive or solenoidal contributions respectively. Figure 5 shows Run S05 as an example. One can see that these terms vary at early times and approach zero asymptotically. This indicates that global exchange between

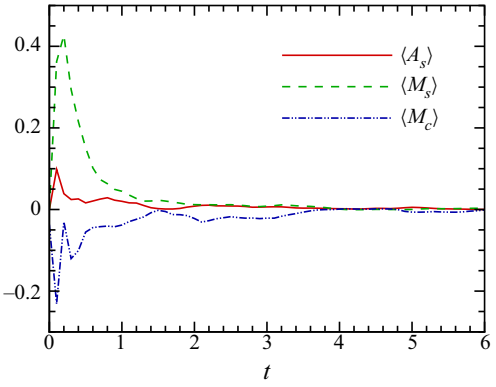


Figure 5. Time variations of the solenoidal part of the advection term $\langle A_s \rangle$ and the solenoidal and compressive part of the Lorentz force term $\langle M_s \rangle$ and$\langle M_c \rangle$ in Run S05 as an example.

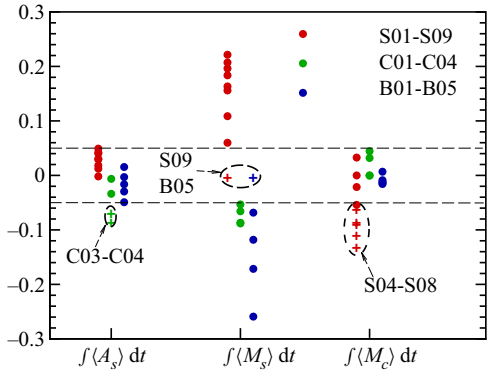


Figure 6. Time integrals (from $t = 0$ to the end of runs) of the advection term $\langle A_s \rangle$ and the solenoidal and compressive parts of the Lorentz force term $\langle M_s \rangle$ and $\langle M_c \rangle$ for all type S, C and B runs.

kinetic and magnetic energy is negligible after adjustments that occur during the first few characteristic times.

Figure 6 shows the time integrals of the advection term and the solenoidal and compressive parts of the Lorentz force term for all the examined runs. Note that the integral, denoted by $\int \cdot \, \mathrm{d}t$, is taken from $t = 0$ to the end of runs, i.e. $t = 10.0$ in our code unit. For most of the runs, a prominent feature is the dominance of the solenoidal part of the Lorentz force term $\int \langle M_s \rangle \, \mathrm{d}t$, accounting for the energy exchange between solenoidal kinetic and magnetic components. One can see that values of the advection term $\int \langle A_s \rangle \, \mathrm{d}t$, and the compressive part of the Lorentz force term $\int \langle M_c \rangle \, \mathrm{d}t$, mainly reside in the range $[-0.05, 0.05]$, while the magnitude of the solenoidal part $\int \langle M_s \rangle \, \mathrm{d}t$ is primarily larger than 0.05. To clarify this point quantitatively, we list these values for some runs in table 3. For example, in Run S01, $\int \langle M_s \rangle \, \mathrm{d}t = 0.16$ and $\int \langle M_c \rangle \, \mathrm{d}t = 0.033$ indicates that a larger fraction of released magnetic energy is converted into solenoidal kinetic energy, as opposed to compressive kinetic energy. Similarly in Run B01, $\int \langle A_s \rangle \, \mathrm{d}t = -0.049$ and $\int \langle M_s \rangle \, \mathrm{d}t = -0.26$ indicates that solenoidal kinetic energy is mainly converted into magnetic energy, while less is converted into compressive kinetic energy. In Run S05, magnetic energy is the main contributor to solenoidal kinetic energy. Conversely, run B03 indicates that solenoidal kinetic energy is the main contributor to magnetic energy. Taken together these runs also support the aforementioned conjecture, that conversion between magnetic energy and flow kinetic energy occurs more readily through couplings

| Run | $\langle E_{k,s}\rangle_0$ | $\langle E_{k,c}\rangle_0$ | $\langle E_b\rangle_0$ | $\int\langle A_s\rangle\,\mathrm{d}t$ | $\int\langle M_s\rangle\,\mathrm{d}t$ | $\int\langle M_c\rangle\,\mathrm{d}t$ |
|---|---|---|---|---|---|---|
| S01 | 0.00 | 0.00 | 0.50 | −0.0018 | 0.16 | 0.033 |
| B01 | 0.50 | 0.00 | 0.025 | −0.049 | −0.26 | 0.0068 |
| S05 | 0.00 | 0.50 | 0.50 | 0.049 | 0.22 | −0.13 |
| B03 | 0.25 | 0.25 | 0.025 | −0.016 | −0.12 | −0.014 |
| B05 | 0.00 | 0.50 | 0.025 | 0.015 | −0.0022 | −0.012 |
| C02 | 0.50 | 0.00 | 0.50 | −0.034 | −0.088 | 0.044 |

Table 3. Selected Runs discussed in Section V. Initial solenoidal kinetic, compressive kinetic and magnetic energy $\langle E_{k,s}\rangle_0$, $\langle E_{k,c}\rangle_0$, $\langle E_b\rangle_0$ and time integrals of the solenoidal part of the advection term $\int\langle A_s\rangle\,\mathrm{d}t$ and the solenoidal and compressive parts of the Lorentz force term $\int\langle M_s\rangle\,\mathrm{d}t$ and $\int\langle M_c\rangle\,\mathrm{d}t$.

that involve the solenoidal part of the flow. There is no clear trend of the relative strength of the compressible kinetic-magnetic exchange $\int\langle M_c\rangle\,\mathrm{d}t$ and the solenoidal-compressive kinetic exchange $\int\langle A_s\rangle\,\mathrm{d}t$, as shown in figure 6; see also Runs B05 and C02 in table 3.

The outliers are marked by crosses in figure 6, which may seem at first to be in conflict with the point above. But it is maybe not so surprising as we look into these simulations. We take Run B05 as an example, whose $\int\langle M_s\rangle\,\mathrm{d}t$ is rather small. Note that neither solenoidal kinetic energy nor a large amount of magnetic energy was introduced initially in Run B05, for which it is reasonable to expect that the interaction between solenoidal kinetic and magnetic components through $\int\langle M_s\rangle\,\mathrm{d}t$ is negligible. With these specific cases in mind, we can make the point that the solenoidal kinetic-magnetic exchange is more efficient than two other available channels, i.e. the solenoidal-compressive kinetic exchange and the compressive kinetic-magnetic exchange. Evidently the interactions of the magnetic field with the compressive flows are mainly oscillatory, in the sense of magnetosonic modes, and tend to rapidly average to small values. The stronger, more secular changes in the energy balance with the magnetic field are mediated more effectively by the solenoidal flow.

## 6. Short-time energy amplification

While energy decay has been previously studied in the context of hydrodynamic and magnetohydrodynamic turbulence, a common feature among many of these studies is the focus on long time asymptotic behaviours. In this section, we instead describe global turbulent processes operating on short time scales. Point-wise relaxation at short time scales has been discussed in Servidio, Matthaeus & Dmitruk (2008).

### 6.1. *Solenoidal kinetic energy amplification*

Note that no solenoidal kinetic energy is initially excited in the series of Type S runs. One may anticipate that a certain amount of solenoidal kinetic energy may be developed at some later time. Indeed, it is reported in Stribling & Matthaeus (1991) that the incompressible MHD system in which kinetic and magnetic energies are initially of greatly different magnitudes can evolve rapidly towards near-equipartition of kinetic and magnetic energies. This tendency towards order-one equipartition is sometimes called the ‘Alfvén effect’ (Fyfe, Montgomery & Joyce 1977) and is widely invoked in astrophysics. For the compressible MHD system presented here, figure 7 shows the time evolution of solenoidal kinetic energy. One can see that the solenoidal kinetic energy $\langle E_{k,s}\rangle$ grows rapidly in each

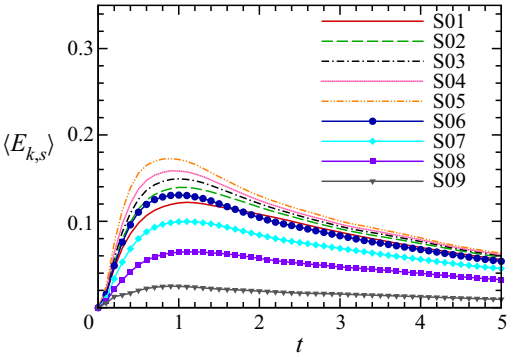


Figure 7. Time variation of solenoidal kinetic energy in type S runs, which initially lack solenoidal flows.

| Run | $\langle E_{k,s}\rangle_0$ | $\langle E_{k,c}\rangle_0$ | $\langle E_b\rangle_0$ | $t_{max}$ | $\langle E_{k,s}\rangle_{t_{max}}$ | $\langle E_{k,c}\rangle_{t_{max}}$ | $\langle E_b\rangle_{t_{max}}$ |
|---|---|---|---|---|---|---|---|
| S01 | 0.00 | 0.00 | 0.50 | 1.1 | 0.122 | 0.0202 | 0.289 |
| S02 | 0.00 | 0.15 | 0.50 | 1.0 | 0.139 | 0.0574 | 0.315 |
| S03 | 0.00 | 0.25 | 0.50 | 1.0 | 0.149 | 0.0758 | 0.327 |
| S04 | 0.00 | 0.35 | 0.50 | 0.9 | 0.158 | 0.103 | 0.345 |
| S05 | 0.00 | 0.50 | 0.50 | 0.9 | 0.173 | 0.125 | 0.361 |
| S06 | 0.00 | 0.50 | 0.35 | 1.0 | 0.130 | 0.118 | 0.268 |
| S07 | 0.00 | 0.50 | 0.25 | 1.1 | 0.0997 | 0.112 | 0.201 |
| S08 | 0.00 | 0.50 | 0.15 | 1.1 | 0.0648 | 0.118 | 0.131 |
| S09 | 0.00 | 0.50 | $1.00 \times 10^{-4}$ | 0.9 | 0.0248 | 0.145 | $1.65 \times 10^{-4}$ |

Table 4. Runs discussed in § 6.1. Initial solenoidal kinetic, compressive kinetic and magnetic energy $\langle E_{k,s}\rangle_0$, $\langle E_{k,c}\rangle_0$, $\langle E_b\rangle_0$, time for $\langle E_{k,s}\rangle$ to reach maximum $t_{max}$, and solenoidal kinetic, compressive kinetic and magnetic energy at $t_{max}$.

type S run, even though it is absent initially, and reaches its maximum at different levels before decay begins.

The time for $\langle E_{k,s}\rangle$ to reach maximum, $t_{max}$, is listed in table 4. For each of the runs, $t_{max} \sim 1$, which is smaller than initial large-eddy turnover time. The maxima of solenoidal kinetic energy are plotted in figure 8 as a function of initial compressive kinetic or magnetic energies for all type S runs. Two branches appear, one (top branch) with fixed $\langle E_b\rangle_0 = 0.5$ and varying $\langle E_{k,c}\rangle_0$ from 0.0 to 0.5, and the other (bottom branch) with fixed $\langle E_{k,c}\rangle_0 = 0.5$ and varying $\langle E_b\rangle_0$ from 0.0 to 0.5. There are at least three points that we can make based on the behaviour shown in figure 8. First, and consistent with intuition, increasing compressive kinetic or magnetic energy can drive more solenoidal kinetic energy. Second, the bottom branch is much steeper than the top branch, while the maximum solenoidal kinetic energy in the top one is always higher than that in the bottom one, suggesting that solenoidal kinetic energy is more efficiently excited by magnetic energy. This recalls the dominance of the solenoidal part of the Lorentz force term $\int \langle M_s\rangle \, \mathrm{d}t$ discussed in § 5. Finally, and perhaps most surprisingly, both branches exhibit nearly linear fits. The linear least-squares fit of top branch yields

$$\langle E_{k,s}\rangle_{t_{max}} = 0.101\langle E_{k,c}\rangle_0 + 0.123, \tag{6.1}$$

and bottom branch yields

$$\langle E_{k,s}\rangle_{t_{max}} = 0.300\langle E_b\rangle_0 + 0.0234. \tag{6.2}$$

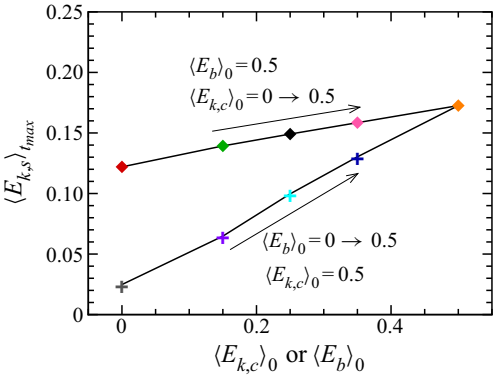


Figure 8. Maximum of solenoidal kinetic energy $\langle E_{k,s}\rangle_{t_{max}}$ as a function of initial compressive kinetic $\langle E_{k,c}\rangle_0$ (diamonds) and magnetic energy $\langle E_b\rangle_0$ (crosses) for type S runs. The arrows indicate increasing initial compressive kinetic and magnetic energy.

We make no claims of universality of the parameters in the linear fits, since only a limited range of initial conditions and parameters are simulated here. For example, $M_t \leqslant 1.0$ in all type S runs, but the Mach number inevitably has impact on the exchange between solenoidal and compressive kinetic energy. Meanwhile, we defer to a future work to explore in detail the reasons for which these linear variations fit well.

#### 6.1.1. *Transition to MEC state*

Recall that the set of type S runs was initiated with pure longitudinal velocity, i.e. compressive wave (CW) state. In such cases, vorticity can be generated via non-baroclinic effects, viscous interactions and the Lorentz force. The S09 run has the smallest solenoidal kinetic energy excited initially and maintains the domination of waves over vortical motions for all times. As shown in figure 9, the ratio of longitudinal velocity ($u_L$) to transverse velocity ($u_T$) is about 2, which clearly lies outside the realm of the NI theory. Also shown is the density variation $\delta\rho = \sqrt{\langle(\rho - \langle\rho\rangle)^2\rangle}$ scaling as $M_t$, suggesting a modally equipartitioned compressive (MEC) density scaling. This is confirmed even more clearly in S05 run, that $\delta\rho/M_t = O(1)$ and $u_L/u_T = O(1)$ since a larger amount of solenoidal kinetic energy is received from magnetic energy. Other type S runs (not shown here) support the conjecture as well that the nearly incompressible state can never be approached in these cases, and the breakdown of CW turbulence leads to a state describable by MEC turbulence.

### 6.2. *Magnetic energy amplification*

The turbulent dynamo is an important process to amplify dynamically the magnetic energy over short time scales. The series B runs have initial magnetic energies of small magnitude and ratios of solenoidal to compressive kinetic energy that range from 0.0 to 1.0. These runs exhibit a rapid amplification of magnetic energy as illustrated in figure 10. We immediately observe that these runs reach maximum values over time at different levels. One can reason in the same way as solenoidal kinetic energy amplification in § 6.1: the solenoidal kinetic-magnetic energy exchange channel via the Lorentz force term $\int\langle M_s\rangle\,\mathrm{d}t$ is more efficient than the compressive-magnetic exchange, thus facilitating the growth of magnetic energy with an increasing solenoidal kinetic energy component.

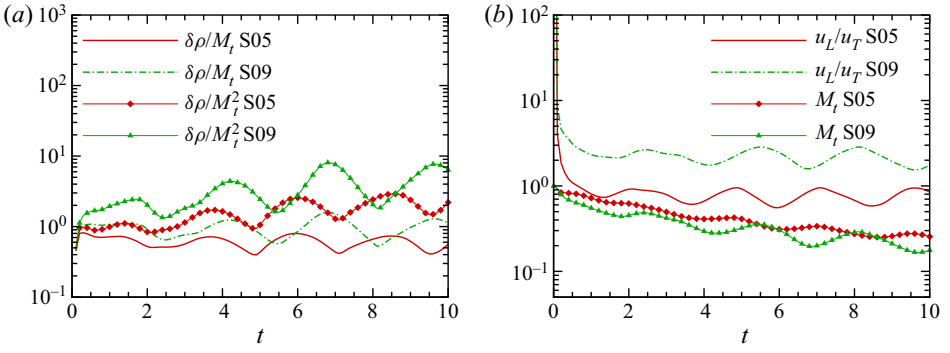


Figure 9. Time histories of $\delta\rho/M_t$, $\delta\rho/M_t^2$, $u_L/u_T$ and $M_t^2$ for S05 and S09 runs.

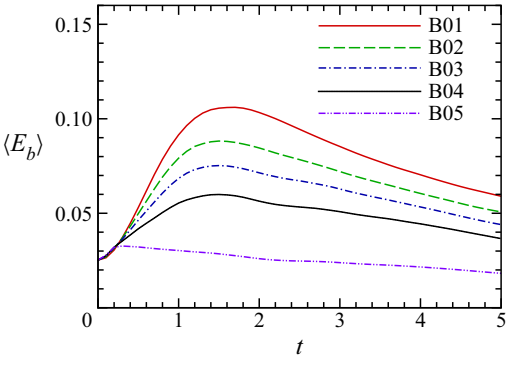


Figure 10. Time variation of magnetic energy in type B runs.

To quantify the contribution to magnetic field amplification from different velocity components, a series of incompressible runs labelled as type I are introduced as listed in table 5. This is quantitatively shown in figure 11, where we plot the maxima of magnetic energy as a function of initial solenoidal kinetic energy for all type B and type I runs. Both compressible and incompressible runs show a strong dependence of the growth rate on the intensity of the initial solenoidal velocity component. The small discrepancy between the maxima of magnetic energy in the compressible simulations and the incompressible simulations is suggestive of the central role of the solenoidal component, namely magnetic energy derives most of its growth from solenoidal kinetic energy as compared with compressive kinetic energy. The result shown here reconciles with the conclusion in Federrath *et al.* (2011) that strong magnetic fields are generated even in purely compressively driven turbulence, but solenoidal turbulence drives more efficient dynamos, due to the higher level of vorticity generation. Proceeding as in § 6.1, the solid lines in figure 11 are fits with

$$\langle E_b \rangle_{t_{max}} = 0.146 \langle E_{k,s} \rangle_0 + 0.0359 \tag{6.3}$$

for the compressible runs and

$$\langle E_b \rangle_{t_{max}} = 0.209 \langle E_{k,s} \rangle_0 + 0.0320 \tag{6.4}$$

for the incompressible runs. We emphasize that the fits do not necessarily reflect a universal behaviour. More cases with different Mach numbers and initial configurations have to be investigated.

| Run | $\langle E_{k,s}\rangle_0$ | $\langle E_{k,c}\rangle_0$ | $\langle E_b\rangle_0$ | $t_{max}$ | $\langle E_{k,s}\rangle_{t_{max}}$ | $\langle E_{k,c}\rangle_{t_{max}}$ | $\langle E_b\rangle_{t_{max}}$ |
|---|---|---|---|---|---|---|---|
| B01 | 0.50 | 0.00 | 0.025 | 1.7 | 0.246 | 0.0168 | 0.106 |
| B02 | 0.35 | 0.15 | 0.025 | 1.5 | 0.187 | 0.0447 | 0.0882 |
| B03 | 0.25 | 0.25 | 0.025 | 1.5 | 0.139 | 0.0609 | 0.0752 |
| B04 | 0.15 | 0.35 | 0.025 | 1.5 | 0.0929 | 0.0765 | 0.0599 |
| B05 | 0.00 | 0.50 | 0.025 | 0.3 | 0.0151 | 0.224 | 0.0327 |
| I01 | 0.50 | — | 0.025 | 1.6 | 0.273 | — | 0.135 |
| I02 | 0.35 | — | 0.025 | 1.7 | 0.196 | — | 0.107 |
| I03 | 0.25 | — | 0.025 | 1.8 | 0.143 | — | 0.0856 |
| I04 | 0.15 | — | 0.025 | 2.1 | 0.0853 | — | 0.0618 |

Table 5. Description of runs discussed in § 6.2. Initial solenoidal kinetic, compressive kinetic and magnetic energy $\langle E_{k,s}\rangle_0$, $\langle E_{k,c}\rangle_0$, $\langle E_b\rangle_0$, time for $\langle E_b\rangle$ to reach maximum $t_{max}$, solenoidal, compressive kinetic and magnetic energy at $t_{max}$.

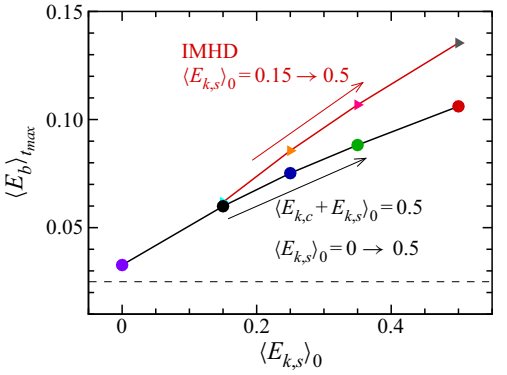


Figure 11. Maximum of magnetic energy $\langle E_b\rangle_{t_{max}}$ as a function of initial solenoidal kinetic energy $\langle E_{k,s}\rangle_0$ for type B compressible runs (circles) and type I incompressible runs (triangles). The arrows indicate increasing initial solenoidal kinetic energy.

### 6.3. *Compressive kinetic energy amplification*

The type C runs, described in table 6, were begun from purely solenoidal velocity, and with turbulent Mach numbers ranging from 0.1 to 2.0. Figure 12 illustrates the time evolution of the compressive kinetic energy for these cases. For run C01, with a low initial turbulent Mach number $M_t = 0.1$, the compressive component remains negligible. With higher initial turbulent Mach number, larger growth is observed, i.e. for runs C02 and C03. No magnetic energy was introduced initially in run C04. So the smaller magnitude of compressive kinetic energy in run C04 relative to run C02 is due to the fact that there is no additional reservoir of energy other than the solenoidal kinetic energy. One observable feature is that this process is faster than the other two (solenoidal kinetic and magnetic) amplification processes described in the previous two sub-sections.

#### 6.3.1. *Longevity of NI state*

A main point of interest is to examine the manner in which the flow eventually departs from the orderings expected in nearly incompressible (NI) theory. One might anticipate that the case C01 with $M_t = 0.1$ is nearly incompressible since vanishing compressive velocity is excited initially. However, the NI picture suggested by the low Mach number

| Run | $M_t$ | $\langle E_{k,s}\rangle_0$ | $\langle E_{k,c}\rangle_0$ | $\langle E_b\rangle_0$ | $t_{max}$ | $\langle E_{k,s}\rangle_{t_{max}}$ | $\langle E_{k,c}\rangle_{t_{max}}$ | $\langle E_b\rangle_{t_{max}}$ |
|---|---|---|---|---|---|---|---|---|
| C01 | 0.1 | 0.50 | 0.00 | 0.50 | 1.2 | 0.346 | $7.27 \times 10^{-4}$ | 0.507 |
| C02 | 1.0 | 0.50 | 0.00 | 0.50 | 0.4 | 0.407 | 0.0416 | 0.469 |
| C03 | 2.0 | 0.50 | 0.00 | 0.50 | 0.2 | 0.453 | 0.0624 | 0.458 |
| C04 | 1.0 | 0.50 | 0.00 | $1.00 \times 10^{-4}$ | 1.2 | 0.390 | 0.0236 | $8.41 \times 10^{-4}$ |

Table 6. Details of Runs discussed in § 6.3. Initial turbulent Mach number $M_t$, initial solenoidal kinetic, compressive kinetic and magnetic energy $\langle E_{k,s}\rangle_0$, $\langle E_{k,c}\rangle_0$, $\langle E_b\rangle_0$, time for $\langle E_{k,c}\rangle$ to reach maximum $t_{max}$, solenoidal kinetic, compressive kinetic and magnetic energy at $t_{max}$.

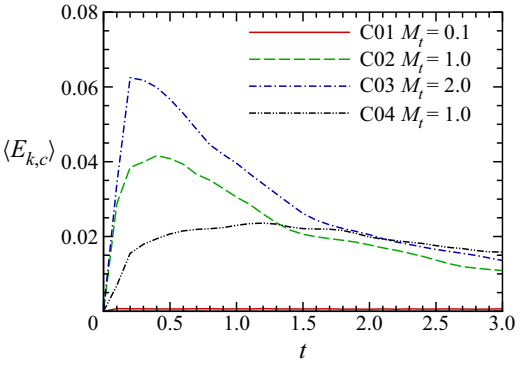


Figure 12. Time variation of compressive kinetic energy in type C runs with varying turbulent Mach numbers.

asymptotic theory of Klainerman & Majda (1981, 1982) cannot remain valid all the time, even in our low Mach number simulations. Although the density fluctuations $\delta\rho$ are of order $M_t^2$ at early time, shown in figure 13, the values of $\delta\rho/M_t^2$ increase above unity quickly, suggesting a trend towards the breakdown of NI picture, as anticipated by Klainerman & Majda (1981, 1982). The ratio of longitudinal to transverse velocity $u_L/u_T$ in figure 13 remains as well roughly consistent with $O(M_t)$ at early time for run C01. For run C02, at higher Mach number, low values of $u_L/u_T$ at early times suggest a transient period of NI behaviour, which gives way to more MEC-like behaviour at later times as this ratio approaches unity. For example, at $t = 15$ in run C02, $u_L/u_T = 0.484$ while $M_t = 0.15$. Although compressive modes are excited by solenoidal kinetic and magnetic components, they are not strong enough to break down NI scaling which can persist for a few characteristic times. Thereafter the system evolves towards MEC characteristics in the presence of non-negligible compressive effects. We recall that, as suggested in Ghosh & Matthaeus (1992), a constant density initial condition is actually a composite state composed of pseudo-sound density fluctuations and identical out-of-phase acoustic fluctuations. Therefore, the presence of acoustic waves in the initial data eventually drive the system away from the NI picture. This occurs more quickly for larger Mach number cases as well, as expected from the formal theory of nearly incompressible flows (Klainerman & Majda 1982).

### 6.3.2. *Comparison with results from spacecraft observations*

The interpretation that the present results, for low Mach number cases, show a dynamical evolution from a $\delta\rho = O(M_t^2)$ ordering to a noisier $\delta\rho = O(M_t)$ ordering at later times is

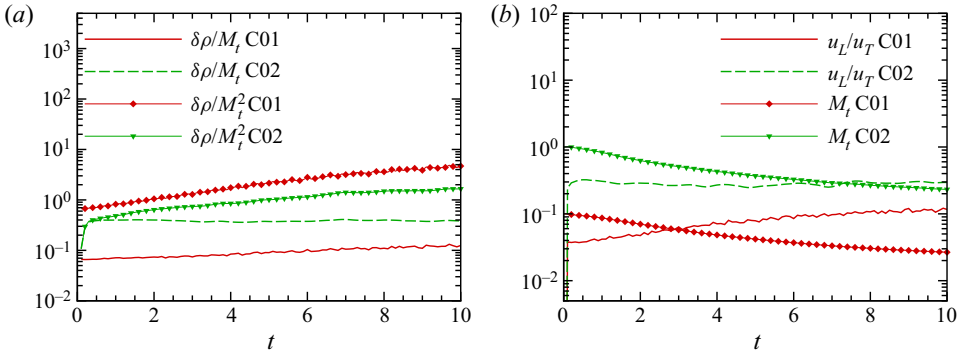


Figure 13. Time histories of $\delta\rho/M_t$, $\delta\rho/M_t^2$, $u_L/u_T$ and $M_t$ for C01 and C02 runs. The C03 and C04 runs give rise to behaviour very similar to the C02 run.

generally consistent with the Klainerman & Majda (1982) picture, but we emphasize that this cannot be viewed as a firm conclusion based on the limited available evidence we have in hand. A complementary, and completely independent, direction where one might find guidance is in the voluminous spacecraft observations of density fluctuations and related quantities in the solar wind (see, e.g. Tu & Marsch (1995), Bruno & Carbone (2013) for a review.)

Joint distributions (scatter plots) of turbulent Mach number and density fluctuations of Voyager observations between 1 and 5 AU heliocentric distances were examined in Matthaeus *et al.* (1991). These results, like the present simulations, supported either $O(M_t)$ or $O(M_t^2)$ scaling, and scaling close to the latter nearly incompressible case for very small density fluctuations $\delta\rho/\rho < 0.01$. Similar analyses were carried out using Helios spacecraft. Grappin, Velli & Mangeney (1991) found $\delta\rho/\rho \simeq M_t^2$ in low-speed wind and $\delta\rho/\rho \simeq 0.1M_t^2$ in high-speed wind. Tu & Marsch (1994) used more than 3000 one hour samples in the distance range 0.29 AU to 1.0 AU. Results were again that observed scalings were ambiguous in their support both for $O(M_t)$ and $O(M_t^2)$ scalings of density. This study delved further into the subject by examining several different formulations of the Mach number, and by also considering an alternative formulation of the NI theory in terms of pressure fluctuations. Klein *et al.* (1993) and Bavassano & Bruno (1995) concluded that there was not strong support for NI theory, or perhaps more accurately, that the theory that predicts $O(M_t^2)$ scaling cannot be unambiguously distinguished from the acoustic wave dominated case. Cited for potential explanation is the variability of external parameters other than Mach number, and in particular the variation of values of plasma $\beta$ (see following section.) Klein *et al.* (1993), Bavassano, Bruno & Klein (1995) and Bavassano, Pietropaolo & Bruno (2004) provided still another look at this problem, now taking into account further subtleties in the MHD approach to near-incompressibility including the possibility of approximate pressure balance due to density-temperature anticorrelations (Zank, Matthaeus & Klein 1990).

Without regard for density fluctuations, compressive fluctuations are often characterized in terms of the ratio of magnetic power in fluctuations perpendicular to the mean magnetic field to that parallel to the mean magnetic field (the so-called variance anisotropy or magnetic compressibility). Smith, Vasquez & Hamilton (2006) and Pine *et al.* (2020) using Voyager and Advanced Composition Explorer (ACE) data show that the variance anisotropy is strongly correlated to the proton beta, which was recast into a form inferring a turbulence Mach number dependence. This may be consistent with the predictions of

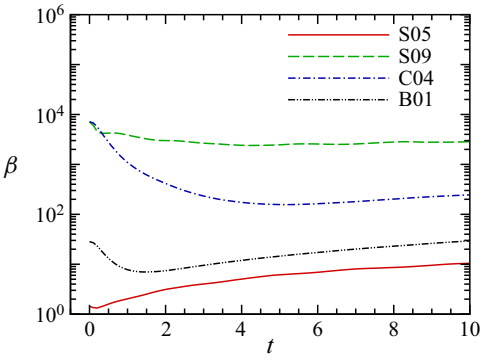


Figure 14. Time histories of $\beta$.

theory and simulation, but we lack a mean guide magnetic field in our simulations to make a reliable comparison.

In this, and for all such solar wind studies that we have found, we see no clear evidence for any single scaling of density with turbulent Mach number. One may recall that the nearly incompressible theory (Zank & Matthaeus 1992) has been formulated in homogeneous background. However, complexities of solar wind could introduce significant complications in the nearly incompressible description of turbulence. For example, the density fluctuations were shown to be of the order of the turbulence Mach number in the presence of a large-scale inhomogeneous background, such as a spatially varying magnetic field (Bhattacharjee *et al.* 1998) and a radially symmetric (magnetic field, velocity and density) background (Hunana & Zank 2010). Recently, Adhikari *et al.* (2020) evaluated the $O(M_t)$ scaling of density fluctuations observed by PSP using SWEAP data during slow solar wind encounters. We return to this topic in the discussion section.

## 7. Behaviour of $\beta$

In the context of MHD the parameter $\beta$

$$\beta = \frac{2p}{B^2} \sim \frac{c_s^2}{V_A^2} \tag{7.1}$$

plays a role in regulating details of the approach to incompressibility, and the nature of the anisotropy that appears dynamically in the presence of a large scale uniform magnetic field (Zank & Matthaeus 1990, 1992). Note that in (7.1), $V_A = B/\sqrt{4\pi\rho}$ is the Alfvén speed. In MHD, $\beta$ also controls activity such as parametric instability of Alfvén waves (Fu *et al.* 2018). The same parameter $\beta$ is of particular importance in plasma descriptions that go beyond a simple fluid closure. A familiar example is the control that plasma $\beta$ exerts over regimes of various plasma instabilities in the solar wind such as firehose, cyclotron and mirror mode instabilities (Gary *et al.* 2001; Maruca *et al.* 2013). We do not investigate such instabilities here, but simply document that typical behaviour of $\beta$ as the turbulence decays in a selected set of our runs.

The time dependence of $\beta$ for selected runs is shown in figure 14. Here we note that the expected behaviour for a large variety of parameters in Type T, S and C runs is that $\beta$ gradually increases with time, as run S05 shown in figure 14. This follows from the increase of pressure, as turbulence decay progressively increases the internal energy, while

at the same time the decrease of fluctuation energy is usually accompanied by decrease in average magnetic pressure. The only exceptions are runs S09, C04 and Type B, which are initiated with very low levels of magnetic energy. In these cases the initial stretching of magnetic field lines and associated magnification of magnetic energy overcomes the initial increase of pressure. In general this type of behaviour would not be expected in cases with significant levels of magnetic energy. For special circumstances plasma $\beta$ might decrease at longer times, for example if a mechanism for cooling is included (see e.g. Yang *et al.* 2016*a*), or if the parameters (such as magnetic helicity) are chosen so that during decay there is appreciable dynamo action.

## 8. Conclusions and discussions

Most classical turbulence theory treats the incompressible case in particular, and this emphasis has carried over to the development of principles and simulations of turbulence in the magnetohydrodynamic case. In gas dynamics there have been great strides in understanding additional effects associated with compressibility, as seen for example in seminal works on low Mach number, weakly compressible flows (Klainerman & Majda 1981, 1982), as well as high Mach number strongly compressive flows. There has also been substantial and growing interest in compressible MHD turbulence, often in the context of dynamo theory and astrophysical flows (Mac Low & Klessen 2004; Brandenburg & Subramanian 2005; Federrath *et al.* 2014).

In the present paper we have concentrated on a basic issue in the physics of compressible MHD turbulence, namely the exchange of energy between different forms during energy decay. In particular our goal has been to refine the understanding of energy exchanges between solenoidal velocity, irrotational velocity, magnetic field fluctuations and thermal energy. Our studies have arrived at several clear conclusions. First, acoustic waves are responsible to the oscillatory exchange between compressive kinetic and thermal energy through the pressure dilatation term; second, Energy exchange between solenoidal kinetic energy and magnetic energy usually dominates over other channels. Finally, the energy amplification rate of different components systematically depends on the initial energy budget. These results afford a certain degree of predictive power, even though the flow could be initialized with highly varied energy configurations. For example, short-time dynamical fate of an arbitrary set of initial data is controlled, to a great extent, by the interchange between solenoidal kinetic and magnetic energy. In order to drive more solenoidal kinetic energy or magnetic energy, the strategy of choice is to initialize with more magnetic energy or solenoidal kinetic energy, instead of adding more compressive kinetic energy.

This paper has maintained a focus on conversion between energy types in decaying compressible MHD turbulence, and as such we have not delved into subjects that are related to various aspects of our study. There are, of course, numerous studies of compressible hydrodynamics that examine turbulence cascade properties; many of these are numerical, as in recent examples by Wang *et al.* (2013, 2019); in total these are far too numerous to review here, and we refer the reader to our reference list and the bibliographies contained therein. The present study of energy balance and conversion between incompressive energy reservoirs and compressive energy reservoirs in MHD is necessarily a richer subject than the numerous analogous studies in hydrodynamics (Kida & Orszag 1990, 1992; Miura & Kida 1995; Pan & Johnsen 2017). The major difference of course is the presence of a dynamically relevant magnetic field in MHD and several new parameters associated with it. In particular the ratio of energy in flows and magnetic fields becomes important, in supplementing the ratio of incompressive and compressive

flows energy which is important in both hydrodynamics and MHD. Additionally the plasma $\beta$ or ratio of thermal pressure to magnetic pressure provides another measure of energy content that influences MHD evolution. All of these factors in principle can influence energy conversion into compressive modes and into thermal energy in ways not present in hydrodynamics. One may note that the oscillatory exchanges between compressive kinetic and thermal energies are attributed to acoustic waves as explained in § 4, which does not differ from hydrodynamics in this sense. However, the actual mode underlying this process is magnetosonic wave. The Alfvén speed is much smaller than the sound speed in our cases, thus merely introducing minor effects on the wavelike character. We anticipate that a stronger magnetic field should allow this point to be distinguished.

Another major issue that we studied here is the relationship of the compressive and incompressive degrees of freedom in MHD. One aspect of that relationship is the approach of the compressible MHD system to the incompressible state, a subject that can be studied using more or less rigorous theoretical approaches that are valid at different values of plasma $\beta$ (Matthaeus & Brown 1988; Zank & Matthaeus 1993; Bhattacharjee *et al.* 1998; Hunana & Zank 2010). Rather than pursue a formal evaluation of theory we opted for a more heuristic study, emphasizing the relationship of the computations to solar wind observations. Our main finding in this regard is that the predicted scaling of density with turbulent Mach number varies between $\delta\rho = O(M_t^2)$ and $\delta\rho = O(M_t)$, apparently as a function of time in these initial values problems. The transition is not sharp. Consequently, one may argue that the main theoretical expectations are observed, approximately, but distinguishing between them in a given case may be an imprecise exercise. We then presented a short summary of observations in the solar wind that had the same goals of distinguishing these scalings. And similar to our results, the solar wind studies also conclude that the data are most often consistent with both $O(M_t)$ and $O(M_t^2)$ scalings, while some find no clear relationship between the density fluctuations and the turbulent Mach number.

We should point out that the methods of identification in the present numerical experiments and the solar wind observational cases are rather different. The computations are controlled initial value problems and we see a 'soft' transition between these scalings. In the solar wind observations it is not possible to follow a parcel of plasma as its dynamics unfold, and therefore all results of this type are purely statistical. The dynamical age of such solar wind parcels can be only crudely estimated. Meanwhile, our simulations have many limitations and might fail to reproduce any particular event. Nevertheless, the two types of studies show a similar level of ambiguity in determining the degree to which the nearly incompressible theoretical description is relevant in general for low Mach number compressible magnetofluids. In this regard we note that it may be possible to establish approximate validity of a 'noisier' version of nearly incompressible theory (see Majda & Embid 1998) which accounts for the utility of concepts from incompressible theory in low Mach number MHD, even if the formal $O(M_t^2)$ scaling of density fluctuations is not strictly valid. Such a theory has not been fully developed as far as we are aware; however see Aluie, Li & Li (2012).

We have only touched the surface of spacecraft observation of compressive turbulence, given that this goes well beyond the studies of nearly-incompressible MHD in the solar wind that we discussed above. An observational study of particular relevance and importance in this regard is that of Zank, Nakanotani & Webb (2019), a study that is closely related to the present one in its goals but vastly dissimilar in its approach. The subject is energy conversion in the local interstellar medium examined using direct in situ observations by Voyager. This study employs the available data (density and magnetic

field) to assess conversion between compressive and incompressive motions based on a framework of *mode conversion* in linear MHD theory. Analysis of solar wind fluctuations in terms of incompressive and compressive wave modes has also been presented (Howes *et al.* 2012; Klein *et al.* 2012).

A recent relatively complete survey of solar wind fluctuations and related quantities in different types of solar wind streams has been given by Borovsky, Denton & Smith (2019). Some of solar wind turbulence studies examine its properties in terms of spectra and higher order scalings related to multifractal theory (e.g. Bruno *et al.* 2014; Riazantseva *et al.* 2015; Carbone *et al.* 2018) and the fluctuations of density, velocity and magnetic field and their possible correlations (e.g. Reid & Kontar 2010; Yao *et al.* 2011; Wicks *et al.* 2013). A review of related effects in compressible plasma turbulence as observed in the solar wind is given in Chen (2016). In such studies density fluctuations and compressive behaviour is often associated in observations with polarization anisotropy, i.e. the ratio of variance parallel and perpendicular to the large scale magnetic field (Smith *et al.* 2006; Pine *et al.* 2020), or with the variance of the magnitude of the magnetic field, including its fluctuations. Both of these are considered indicators of compressive activity, in accordance with properties of Alfvén wave solutions either at small or large amplitude (see Barnes 1979). While such studies are of immense value, they are necessarily statistical, as they cannot follow dynamics of specific parcels of plasma and so conversion cannot be explicitly followed as we have done here. Another direction in observational studies of compressive solar wind turbulence follows the development of extensions of the third order cascade law (Politano & Pouquet 1998) to the compressive case (Podesta 2008; Carbone *et al.* 2009; Banerjee & Galtier 2013; Andrés *et al.* 2018). The studies by Banerjee *et al.* (2016*b*), Hadid *et al.* (2017, 2018) and Andrés *et al.* (2019) employ the cascade model and evaluate contributions to the total cascade rate due to both compressive and incompressive channels. While these theories are of great interest, the experimental implementation is hampered by inability of measuring all quantities involved with single spacecraft, as well as limitation of applicability due to the additional approximations adopted (such as constant plasma beta).

Future studies will likely be motivated to examine the effects of a mean guide (DC) magnetic field $B_0$ of varying strength. The effects of such an externally applied field are relatively well understood in the incompressible case. One major influence in that case is the development of spectral anisotropy, and effect induced by the interplay of processes operating at the nonlinear timescales with processes associated with Alfvén propagation. The relatively enhanced propensity to develop strong perpendicular gradients has been well established (Shebalin, Matthaeus & Montgomery 1983; Cho & Lazarian 2003; Oughton *et al.* 2015). However so far the global conversion between different energy reservoirs, as we have done in the present paper, appears not to have been fully addressed with a varying strength guide field. We will take this up in a future study.

**Funding.** This work has been supported by NSFC Grant Nos. 91752201, 11672123 and 11902138; the Shenzhen Science and Technology Innovation Committee (Grant No. KQTD20180411143441009); the Department of Science and Technology of Guangdong Province (Grant No. 2019B21203001) and Key Special Project for Introduced Talents Team of Southern Marine Science and Engineering Guangdong Laboratory (Guangzhou) (GML2019ZD0103). We acknowledge computing support provided by Center for Computational Science and Engineering of Southern University of Science and Technology. W.H.M. is partially supported by NASA HSR grants NNX17AB79G, 80NSSC18K1210, 80NSSC18K1648 and 80NSSC19K0284. S.C. acknowledges support from the National Natural Science Foundation of China Basic Science Center Program (Grant No. 11988102).

**Declaration of interests.** The authors report no conflict of interest.

**Author ORCIDs.**
Minping Wan https://orcid.org/0000-0001-5891-9579;
William H. Matthaeus https://orcid.org/0000-0001-7224-6024.

## Appendix A

The incompressible MHD equations we solve are,

$$\frac{\partial \boldsymbol{u}}{\partial t} + (\boldsymbol{u}\cdot\nabla)\,\boldsymbol{u} = -\nabla p_M + (\boldsymbol{b}\cdot\nabla)\,\boldsymbol{b} + \nu\Delta\boldsymbol{u}, \tag{A1}$$

$$\frac{\partial \boldsymbol{b}}{\partial t} + (\boldsymbol{u}\cdot\nabla)\,\boldsymbol{b} = (\boldsymbol{b}\cdot\nabla)\,\boldsymbol{u} + \eta\Delta\boldsymbol{b}, \tag{A2}$$

$$\nabla\cdot\boldsymbol{u} = 0, \quad \nabla\cdot\boldsymbol{b} = 0, \tag{A3$a$,$b$}$$

where $p_M = p + |\boldsymbol{b}|^2/2$, $\nu$ and $\eta$ denote the total pressure, the kinematic viscosity and the magnetic diffusivity, respectively.

## References

Adhikari, L., *et al.* 2020 Turbulence transport modeling and first orbit parker solar probe (PSP) observations. *Astrophys. J. Suppl.* **246** (2), 38.

Aluie, H. & Eyink, G.L. 2010 Scale locality of magnetohydrodynamic turbulence. *Phys. Rev. Lett.* **104**, 081101.

Aluie, H., Li, S. & Li, H. 2012 Conservative cascade of kinetic energy in compressible turbulence. *Astrophys. J. Lett.* **751**, L29.

Andrés, N., Sahraoui, F., Galtier, S., Hadid, L.Z., Dmitruk, P. & Mininni, P.D. 2018 Energy cascade rate in isothermal compressible magnetohydrodynamic turbulence. *J. Plasma Phys.* **84** (4), 905840404.

Andrés, N., Sahraoui, F., Galtier, S., Hadid, L.Z., Ferrand, R. & Huang, S.Y. 2019 Energy cascade rate measured in a collisionless space plasma with MMS data and compressible Hall magnetohydrodynamic turbulence theory. *Phys. Rev. Lett.* **123** (24), 245101.

Armstrong, J.W., Cordes, J.M. & Rickett, B.J. 1981 Density power spectrum in the local interstellar medium. *Nature* **291** (5816), 561–564.

Bandyopadhyay, R., Matthaeus, W.H., Oughton, S. & Wan, M. 2019 Evolution of similarity lengths in anisotropic magnetohydrodynamic turbulence. *J. Fluid Mech.* **876**, 5–18.

Banerjee, S. & Galtier, S. 2013 Exact relation with two-point correlation functions and phenomenological approach for compressible magnetohydrodynamic turbulence. *Phys. Rev.* E **87**, 013019.

Banerjee, S., Hadid, L.Z., Sahraoui, F. & Galtier, S. 2016*a* Scaling of compressible magnetohydrodynamic turbulence in the fast solar wind. *Astrophys. J. Lett.* **829** (2), L27.

Banerjee, S., Hadid, L.Z., Sahraoui, F. & Galtier, S. 2016*b* Scaling of compressible magnetohydrodynamic turbulence in the fast solar wind. *Astrophys. J. Lett.* **829**, L27.

Barnes, A. 1979 Hydromagnetic waves and turbulence in the solar wind. In *Solar System Plasma Physics, I* (ed. E.N. Parker, C.F. Kennel & L.J. Lanzerotti), p. 251. North-Holland.

Bavassano, B., Bruno, R. & Klein, L.W. 1995 Density-temperature correlation in solar-wind magnetohydrodynamic fluctuations—a test for nearly incompressible models. *J. Geophys. Res.* **100**, 5871–5875.

Bavassano, B., Pietropaolo, E. & Bruno, R. 2004 Compressive fluctuations in high-latitude solar wind. In *Annales Geophysicae*, vol. 22, pp. 689–696. Copernicus GmbH.

Bavassano, R. & Bruno, R. 1995 Density fluctuations and turbulent Mach numbers in the inner solar wind. *J. Geophys. Res.* **100**, 9475–9480.

Bec, J. & Khanin, K. 2007 Burgers turbulence. *Phys. Rep.* **447** (1–2), 1–66.

Benzi, R., Biferale, L., Fisher, R.T., Kadanoff, L.P., Lamb, D.Q. & Toschi, F. 2008 Intermittency and universality in fully developed inviscid and weakly compressible turbulent flows. *Phys. Rev. Lett.* **100** (23), 234503.

Beresnyak, A., Lazarian, A. & Cho, J. 2005 Density scaling and anisotropy in supersonic magnetohydrodynamic turbulence. *Astrophys. J. Lett.* **624** (2), L93.

BHATTACHARJEE, A., NG, C.S., GHOSH, S. & GOLDSTEIN, M.L. 1999 A comparative study of four-field and fully compressible magnetohydrodynamic turbulence in the solar wind. *J. Geophys. Res.* **104** (A11), 24835–24843.

BHATTACHARJEE, A., NG, C.S. & SPANGLER, S.R. 1998 Weakly compressible magnetohydrodynamic turbulence in the solar wind and the interstellar medium. *Astrophys. J.* **494** (1), 409–418.

BIGOT, B., GALTIER, S. & POLITANO, H. 2008 Energy decay laws in strongly anisotropic magnetohydrodynamic turbulence. *Phys. Rev. Lett.* **100** (7), 074502.

BISKAMP, D. & MÜLLER, W.-C. 1999 Decay laws for three-dimensional magnetohydrodynamic turbulence. *Phys. Rev. Lett.* **83** (11), 2195–2198.

BOROVSKY, J.E. 2010 Contribution of strong discontinuities to the power spectrum of the solar wind. *Phys. Rev. Lett.* **105** (11), 111102.

BOROVSKY, J.E., DENTON, M.H. & SMITH, C.W. 2019 Some properties of the solar wind turbulence at 1 AU statistically examined in the different types of solar wind plasma. *J. Geophys. Res.* **124** (4), 2406–2424.

BRANDENBURG, A. & KAHNIASHVILI, T. 2017 Classes of hydrodynamic and magnetohydrodynamic turbulent decay. *Phys. Rev. Lett.* **118** (5), 055102.

BRANDENBURG, A. & LAZARIAN, A. 2013 Astrophysical hydromagnetic turbulence. *Space Sci. Rev.* **178** (2–4), 163–200.

BRANDENBURG, A. & SUBRAMANIAN, K. 2005 Astrophysical magnetic fields and nonlinear dynamo theory. *Phys. Rep.* **417** (1–4), 1–209.

BRUNO, R. & CARBONE, V. 2013 The solar wind as a turbulence laboratory. *Living Rev. Sol. Phys.* **10** (1), 1–208.

BRUNO, R., TELLONI, D., PRIMAVERA, L., PIETROPAOLO, E., D'AMICIS, R., SORRISO-VALVO, L., CARBONE, V., MALARA, F. & VELTRI, P. 2014 Radial evolution of the intermittency of density fluctuations in the fast solar wind. *Astrophys. J.* **786** (1), 53.

BURLAGA, L.F., MISH, W.H. & ROBERTS, D.A. 1989 Large-scale fluctuations in the solar wind at 1 AU: 1978–1982. *J. Geophys. Res.* **94** (A1), 177–184.

CARBONE, F., SORRISO-VALVO, L., ALBERTI, T., LEPRETI, F., CHEN, C.H.K., NĚMEČEK, Z. & ŠAFRÁNKOVÁ, J. 2018 Arbitrary-order hilbert spectral analysis and intermittency in solar wind density fluctuations. *Astrophys. J.* **859** (1), 27.

CARBONE, V., MARINO, R., SORRISO-VALVO, L., NOULLEZ, A. & BRUNO, R. 2009 Scaling laws of turbulence and heating of fast solar wind: the role of density fluctuations. *Phys. Rev. Lett.* **103** (6), 061102.

CELANI, A., LANOTTE, A., MAZZINO, A. & VERGASSOLA, M. 2000 Universality and saturation of intermittency in passive scalar turbulence. *Phys. Rev. Lett.* **84** (11), 2385.

CELANI, A., LANOTTE, A., MAZZINO, A. & VERGASSOLA, M. 2001 Fronts in passive scalar turbulence. *Phys. Fluids* **13** (6), 1768–1783.

CERRETANI, J. & DMITRUK, P. 2019 Coexistence of acoustic waves and turbulence in low mach number compressible flows. *Phys. Fluids* **31** (4), 045102.

CHEN, C.H.K. 2016 Recent progress in astrophysical plasma turbulence from solar wind observations. *J. Plasma Phys.* **82** (6), 535820602.

CHEN, C.H.K., SALEM, C.S., BONNELL, J.W., MOZER, F.S. & BALE, S.D. 2012 Density fluctuation spectrum of solar wind turbulence between ion and electron scales. *Phys. Rev. Lett.* **109** (3), 035001.

CHO, J. & LAZARIAN, A. 2002 Compressibe sub-Alfvén MHD turbulence in low-$\beta$ plasmas. *Phys. Rev. Lett.* **88**, 245001.

CHO, J. & LAZARIAN, A. 2003 Compressible magnetohydrodynamic turbulence: mode coupling, scaling relations, anisotropy, viscosity-damped regime and astrophysical implications. *Mon. Not. R. Astron. Soc.* **345**, 325–339.

ELMEGREEN, B.G. & SCALO, J. 2004 Interstellar turbulence I: observations and processes. *Annu. Rev. Astron. Astrophys.* **42**, 211–273.

FEDERRATH, C., CHABRIER, G., SCHOBER, J., BANERJEE, R., KLESSEN, R.S. & SCHLEICHER, D.R.G. 2011 Mach number dependence of turbulent magnetic field amplification: solenoidal versus compressive flows. *Phys. Rev. Lett.* **107** (11), 114504.

FEDERRATH, C., ROMAN-DUVAL, J., KLESSEN, R.S., SCHMIDT, W. & MAC LOW, M.-M. 2010 Comparing the statistics of interstellar turbulence in simulations and observations-solenoidal versus compressive turbulence forcing. *Astron. Astrophys.* **512**, A81.

FEDERRATH, C., SCHOBER, J., BOVINO, S. & SCHLEICHER, D.R.G. 2014 The turbulent dynamo in highly compressible supersonic plasmas. *Astrophys. J. Lett.* **797** (2), L19.

FU, X., LI, H., GUO, F., LI, X. & ROYTERSHTEYN, V. 2018 Parametric decay instability and dissipation of low-frequency Alfvén waves in low-beta turbulent plasmas. *Astrophys. J.* **855** (2), 139.

FYFE, D., MONTGOMERY, D. & JOYCE, G. 1977 Dissipative, forced turbulence in two-dimensional magnetohydrodynamics. *J. Plasma Phys.* **17**, 369–398.

GALTIER, S., POLITANO, H. & POUQUET, A. 1997 Self-similar energy decay in magnetohydrodynamic turbulence. *Phys. Rev. Lett.* **79** (15), 2807–2810.

GARY, S.P., SKOUG, R.M., STEINBERG, J.T. & SMITH, C.W. 2001 Proton temperature anisotropy constraint in the solar wind: ace observations. *Geophys. Res. Lett.* **28** (14), 2759–2762.

GHOSH, S. & MATTHAEUS, W.H. 1990 Relaxation processes in a turbulent compressible magnetofluid. *Phys. Fluids* B **2** (7), 1520–1534.

GHOSH, S. & MATTHAEUS, W.H. 1992 Low Mach number two-dimensional hydrodynamic turbulence: energy budgets and density fluctuations in a polytropic fluid. *Phys. Fluids* A **4** (1), 148–164.

GOLDSTEIN, B. & SISCOE, G.L. 1972 Spectra and cross spectra of solar wind parameters from mariner 5. *NASA Special Publ.* **308**, 506–516.

GRAPPIN, R., VELLI, M. & MANGENEY, A. 1991 'Alfvénic' versus 'standard' turbulence in the solar wind. *Ann. Geophys.* **9**, 416–426.

GRETE, P., O'SHEA, B.W., BECKWITH, K., SCHMIDT, W. & CHRISTLIEB, A. 2017 Energy transfer in compressible magnetohydrodynamic turbulence. *Phys. Plasmas* **24** (9), 092311.

HADID, L.Z., SAHRAOUI, F. & GALTIER, S. 2017 Energy cascade rate in compressible fast and slow solar wind turbulence. *Astrophys. J.* **838** (1), 9.

HADID, L.Z., SAHRAOUI, F., GALTIER, S. & HUANG, S.Y. 2018 Compressible magnetohydrodynamic turbulence in the earth's magnetosheath: estimation of the energy cascade rate using in situ spacecraft data. *Phys. Rev. Lett.* **120** (5), 055102.

HELLINGER, P., VERDINI, A., LANDI, S., FRANCI, L. & MATTEINI, L. 2018 von Kármán–Howarth equation for Hall magnetohydrodynamics: hybrid simulations. *Astrophys. J. Lett.* **857** (2), L19.

HNAT, B., CHAPMAN, S.C. & ROWLANDS, G. 2005 Compressibility in solar wind plasma turbulence. *Phys. Rev. Lett.* **94** (20), 204502.

HOSSAIN, M., GRAY, P.C., PONTIUS, D.H. JR., MATTHAEUS, W.H. & OUGHTON, S. 1995 Phenomenology for the decay of energy-containing eddies in homogeneous mhd turbulence. *Phys. Fluids* **7**, 2886–2904.

HOWES, G.G., BALE, S.D., KLEIN, K.G., CHEN, C.H.K., SALEM, C.S. & TENBARGE, J.M. 2012 The slow-mode nature of compressible wave power in solar wind turbulence. *Astrophys. J. Lett.* **753** (1), L19.

HUANG, Y.X., SCHMITT, F.G., LU, Z.M., FOUGAIROLLES, P., GAGNE, Y. & LIU, Y.L. 2010 Second-order structure function in fully developed turbulence. *Phys. Rev.* E **82** (2), 026319.

HUNANA, P. & ZANK, G.P. 2010 Inhomogeneous nearly incompressible description of magnetohydrodynamic turbulence. *Astrophys. J.* **718** (1), 148.

IROSHNIKOV, P.S. 1964 Turbulence of a conducting fluid in a strong magnetic field. *Sov. Astron.* **7**, 566–571.

KIDA, S. & ORSZAG, S.A. 1990 Energy and spectral dynamics in forced compressible turbulence. *J. Sci. Comput.* **5**, 85–125.

KIDA, S. & ORSZAG, S.A. 1992 Energy and spectral dynamics in decaying compressible turbulence. *J. Sci. Comput.* **7** (1), 1–34.

KINNEY, R., MCWILLIAMS, J.C. & TAJIMA, T. 1995 Coherent structures and turbulent cascades in two-dimensional incompressible magnetohydrodynamic turbulence. *Phys. Plasmas* **2** (10), 3623–3639.

KLAINERMAN, S. & MAJDA, A. 1981 Singular limits of quasilinear hyperbolic systems with large parameters and the incompressible limit of compressible fluids. *Commun. Pure Appl. Maths* **34** (4), 481–524.

KLAINERMAN, S. & MAJDA, A. 1982 Compressible and incompressible fluids. *Commun. Pure Appl. Maths* **35**, 629–651.

KLEIN, K.G., HOWES, G.G., TENBARGE, J.M., BALE, S.D., CHEN, C.H.K. & SALEM, C.S. 2012 Using synthetic spacecraft data to interpret compressible fluctuations in solar wind turbulence. *Astrophys. J.* **755** (2), 159.

KLEIN, L., BRUNO, R., BAVASSANO, B. & ROSENBAUER, H. 1993 Scaling of density fluctuations with Mach number and density-temperature anticorrelations in the inner heliosphere. *J. Geophys. Res.* **98** (A5), 7837–7841.

KOLMOGOROV, A.N. 1941 The local structure of turbulence in incompressible viscous fluid for very large Reynolds numbers. *Dokl. Akad. Nauk SSSR* **30**, 301–305.

KOWAL, G. & LAZARIAN, A. 2007 Scaling relations of compressible MHD turbulence. *Astrophys. J.* **666**, L67–L72.

KOWAL, G. & LAZARIAN, A. 2010 Velocity field of compressible magnetohydrodynamic turbulence: wavelet decomposition and mode scalings. *Astrophys. Galaxies* **720**, 742–756.

KRAICHNAN, R.H. 1955 On the statistical mechanics of an adiabatically compressible fluid. *J. Acoust. Soc. Am.* **27** (3), 438–441.

KRAICHNAN, R.H. 1965 Inertial-range spectrum of hydromagnetic turbulence. *Phys. Fluids* **8** (7), 1385–1387.
KRITSUK, A.G., WAGNER, R. & NORMAN, M.L. 2013 Energy cascade and scaling in supersonic isothermal turbulence. *J. Fluid Mech.* **729**, R1.
LEE, K., YU, D. & GIRIMAJI, S.S. 2006 Lattice Boltzmann DNS of decaying compressible isotropic turbulence with temperature fluctuations. *Intl J. Comput. Fluid Dyn.* **20** (6), 401–413.
LEMASTER, M.N. & STONE, J.M. 2009 Dissipation and heating in supersonic hydrodynamic and MHD turbulence. *Astrophys. J.* **691** (2), 1092.
LITHWICK, Y. & GOLDREICH, P. 2001 Compressible magnetohydrodynamic turbulence in interstellar plasmas. *Astrophys. J.* **562**, 279–296.
MAC LOW, M.-M. 1999 The energy dissipation rate of supersonic, magnetohydrodynamic turbulence in molecular clouds. *Astrophys. J.* **524** (1), 169–178.
MAC LOW, M.-M. & KLESSEN, R.S. 2004 Control of star formation by supersonic turbulence. *Astrophysics* **76**, 125–194.
MAC LOW, M.-M., KLESSEN, R.S., BURKERT, A. & SMITH, M.D. 1998 Kinetic energy decay rates of supersonic and super-Alfvénic turbulence in star-forming clouds. *Phys. Rev. Lett.* **80** (13), 2754–2757.
MAJDA, A.J. & EMBID, P. 1998 Averaging over fast gravity waves for geophysical flows with unbalanced initial data. *Theor. Comput. Fluid Dyn.* **11**, 155–169.
MAKWANA, K.D. & YAN, H. 2020 Properties of magnetohydrodynamic modes in compressively driven plasma turbulence. *Phys. Rev.* X **10** (3), 031021.
MARUCA, B.A., BALE, S.D., SORRISO-VALVO, L., KASPER, J.C. & STEVENS, M.L. 2013 Collisional thermalization of hydrogen and helium in solar-wind plasma. *Phys. Rev. Lett.* **111**, 241101.
MATTHAEUS, W.H. & BROWN, M.R. 1988 Nearly incompressible magnetohydrodynamics at low Mach number. *Phys. Fluids* **31** (12), 3634–3644.
MATTHAEUS, W.H., KLEIN, L.W., GHOSH, S. & BROWN, M.R. 1991 Nearly incompressible magnetohydrodynamics, pseudosound, and solar wind fluctuations. *J. Geophys. Res.* **96**, 5421–5435.
MININNI, P.D. 2011 Scale interactions in magnetohydrodynamic turbulence. *Annu. Rev. Fluid Mech.* **43**, 377–397.
MIURA, H. & KIDA, S. 1995 Acoustic energy exchange in compressible turbulence. *Phys. Fluids* **7**, 1732–1742.
MOFFATT, H.K. 1978 *Field Generation in Electrically Conducting Fluids*. Cambridge University Press.
MONTGOMERY, D., BROWN, M.R. & MATTHAEUS, W.H. 1987 Density fluctuation spectra in magnetohydrodynamic turbulence. *J. Geophys. Res.* **92** (A1), 282–284.
MONTGOMERY, D., TURNER, L. & VAHALA, G. 1978 Three-dimensional magnetohydrodynamic turbulence in cylindrical geometry. *Phys. Fluids* **21** (5), 757–764.
OUGHTON, S., MATTHAEUS, W.H., WAN, M. & OSMAN, K.T. 2015 Anisotropy in solar wind plasma turbulence. *Phil. Trans. R. Soc. Lond.* A **373**, 20140152.
PADOAN, P. & NORDLUND, Å. 1999 A super-Alfvénic model of dark clouds. *Astrophys. J.* **526** (1), 279–294.
PAN, S. & JOHNSEN, E. 2017 The role of bulk viscosity on the decay of compressible, homogeneous, isotropic turbulence. *J. Fluid Mech.* **833**, 717–744.
PARKER, E.N. 1957 Sweet's mechanism for merging magnetic fields in conducting fluids. *J. Geophys. Res.* **62** (4), 509–520.
PINE, Z.B., *et al.* 2020 Solar wind turbulence from 1 to 45 AU. III. Anisotropy of magnetic fluctuations in the inertial range using voyager and ace observations. *Astrophys. J.* **900** (2), 93.
PODESTA, J.J. 2008 Laws for third-order moments in homogeneous anisotropic incompressible magnetohydrodynamic turbulence. *J. Fluid Mech.* **609**, 171–194.
POLITANO, H. & POUQUET, A. 1998 Von Kármán–Howarth equation for magnetohydrodynamics and its consequences on third-order longitudinal structure and correlation functions. *Phys. Rev.* E **57**, R21–R24.
POUQUET, A., BRACHET, M.-E., LEE, E., MININNI, P., ROSENBERG, D. & URITSKY, V. 2010 Lack of universality in mhd turbulence, and the possible emergence of a new paradigm? *Proc. Intl Astronom. Union* **6** (S271), 304–316.
POUQUET, A., SULEM, P.L. & MENEGUZZI, M. 1988 Influence of velocity-magnetic field correlations on decaying magnetohydrodynamic turbulence with neutral X points. *Phys. Fluids* **31** (9), 2635–2643.
PRATURI, D.S. & GIRIMAJI, S.S. 2019 Effect of pressure-dilatation on energy spectrum evolution in compressible turbulence. *Phys. Fluids* **31** (5), 055114.
PRATURI, D.S. & GIRIMAJI, S.S. 2020 Magnetic–internal–kinetic energy interactions in high-speed turbulent magnetohydrodynamic jets. *Trans. ASME J. Fluids Engng* **142** (10), 101213.
REID, H.A.S. & KONTAR, E.P. 2010 Solar wind density turbulence and solar flare electron transport from the sun to the earth. *Astrophys. J.* **721** (1), 864.

RIAZANTSEVA, M.O., BUDAEV, V.P., ZELENYI, L.M., ZASTENKER, G.N., PAVLOS, G.P., SAFRANKOVA, J., NEMECEK, Z., PRECH, L. & NEMEC, F. 2015 Dynamic properties of small-scale solar wind plasma fluctuations. *Phil. Trans. R. Soc. Lond.* A **373** (2041), 20140146.

RISTORCELLI, J.R. 1997 A pseudo-sound constitutive relationship for the dilatational covariances in compressible turbulence. *J. Fluid Mech.* **347**, 37–70.

ROBERTS, D.A. & GOLDSTEIN, M.L. 1987 Spectral signatures of jumps and turbulence in interplanetary speed and magnetic field data. *J. Geophys. Res.* **92** (A9), 10105–10110.

ROBERTS, O.W., NARITA, Y., LI, X., ESCOUBET, C.P. & LAAKSO, H. 2017 Multipoint analysis of compressive fluctuations in the fast and slow solar wind. *J. Geophys. Res.* **122** (7), 6940–6963.

SALVESEN, G., BECKWITH, K., SIMON, J.B., O'NEILL, S.M. & BEGELMAN, M.C. 2014 Quantifying energetics and dissipation in magnetohydrodynamic turbulence. *Mon. Not. R. Astron. Soc.* **438** (2), 1355–1376.

SARKAR, S. 1992 The pressure-dilatation correlation in compressible flows. *Phys. Fluids* A **4**, 2674–2682.

SCHMIDT, W., FEDERRATH, C. & KLESSEN, R. 2008 Is the scaling of supersonic turbulence universal? *Phys. Rev. Lett.* **101**, 194505.

SERVIDIO, S., MATTHAEUS, W.H. & DMITRUK, P. 2008 Depression of nonlinearity in decaying isotropic MHD turbulence. *Phys. Rev. Lett.* **100**, 095005.

SHEBALIN, J.V., MATTHAEUS, W.H. & MONTGOMERY, D. 1983 Anisotropy in MHD turbulence due to a mean magnetic field. *J. Plasma Phys.* **29**, 525–547.

SHEBALIN, J.V. & MONTGOMERY, D. 1988 Turbulent magnetohydrodynamic density fluctuations. *J. Plasma Phys.* **39** (2), 339–367.

SHODA, M., SUZUKI, T.K., ASGARI-TARGHI, M. & YOKOYAMA, T. 2019 Three-dimensional simulation of the fast solar wind driven by compressible magnetohydrodynamic turbulence. *Astrophys. J. Lett.* **880** (1), L2.

SISCOE, G.L., DAVIS, L. JR., COLEMAN, P.J. JR., SMITH, E.J. & JONES, D.E. 1968 Power spectra and discontinuities of the interplanetary magnetic field: mariner 4. *J. Geophys. Res.* **73** (1), 61–82.

SMITH, C.W., VASQUEZ, B.J. & HAMILTON, K. 2006 Interplanetary magnetic fluctuation anisotropy in the inertial range. *J. Geophys. Res.* **111**, A09111.

SPANGLER, S.R. & SPITLER, L.G. 2004 An empirical investigation of compressibility in magnetohydrodynamic turbulence. *Phys. Plasmas* **11** (5), 1969–1977.

SREENIVASAN, K.R. 1991 On local isotropy of passive scalars in turbulent shear flows. *Proc. R. Soc. Lond.* A **434** (1890), 165–182.

STONE, J.M., OSTRIKER, E.C. & GAMMIE, C.F. 1998 Dissipation in compressible magnetohydrodynamic turbulence. *Astrophys. J. Lett.* **508** (1), L99.

STRIBLING, T. & MATTHAEUS, W.H. 1991 Relaxation processes in a low-order three-dimensional magnetohydrodynamics model. *Phys. Fluids* B **3** (8), 1848–1864.

TAYLOR, J.B. 1974 Relaxation of toroidal plasma and generation of reverse magnetic fields. *Phys. Rev. Lett.* **33** (19), 1139–1141.

TU, C.-Y. & MARSCH, E. 1994 On the nature of compressive fluctuations in the solar wind. *J. Geophys. Res.* **99** (A11), 21481–21509.

TU, C.-Y. & MARSCH, E. 1995 MHD structures, waves and turbulence in the solar wind: observations and theories. *Space Sci. Rev.* **73**, 1–210.

WAN, M., OUGHTON, S., SERVIDIO, S. & MATTHAEUS, W.H. 2012 von Kármán self-preservation hypothesis for magnetohydrodynamic turbulence and its consequences for universality. *J. Fluid Mech.* **697**, 296–315.

WANG, J., GOTOH, T. & WATANABE, T. 2017 Scaling and intermittency in compressible isotropic turbulence. *Phys. Rev. Fluids* **2** (5), 053401.

WANG, J., WAN, M., CHEN, S., XIE, C., LIAN-PING, W. & CHEN, S. 2019 Cascades of temperature and entropy fluctuations in compressible turbulence. *J. Fluid Mech.* **867**, 195–215.

WANG, J., YANG, Y., SHI, Y., XIAO, Z., HE, X.T. & CHEN, S. 2013 Cascade of kinetic energy in three-dimensional compressible turbulence. *Phys. Rev. Lett.* **110** (21), 214505.

WICKS, R.T., MALLET, A., HORBURY, T.S., CHEN, C.H.K., SCHEKOCHIHIN, A.A. & MITCHELL, J.J. 2013 Alignment and scaling of large-scale fluctuations in the solar wind. *Phys. Rev. Lett.* **110** (2), 025003.

YANG, L., ZHANG, L., HE, J., TU, C., LI, S., WANG, X. & WANG, L. 2018 Coexistence of slow-mode and Alfvén-mode waves and structures in 3D compressive MHD turbulence. *Astrophys. J.* **866** (1), 41.

YANG, Y. 2019 Hybrid scheme for compressible MHD turbulence. In *Energy Transfer and Dissipation in Plasma Turbulence*, pp. 35–67. Springer.

YANG, Y., MATTHAEUS, W.H., SHI, Y., WAN, M. & CHEN, S. 2017 Compressibility effect on coherent structures, energy transfer and scaling in magnetohydrodynamic turbulence. *Phys. Fluids* **29**, 035105.

YANG, Y., SHI, Y., WAN, M., MATTHAEUS, W.H. & CHEN, S. 2016*a* Energy cascade and its locality in compressible magnetohydrodynamic turbulence. *Phys. Rev.* E **93**, 061102.

YANG, Y., WAN, M., SHI, Y., YANG, K. & CHEN, S. 2016*b* A hybrid scheme for compressible magnetohydrodynamic turbulence. *J. Comput. Phys.* **306**, 73–91.

YAO, S., HE, J.-S., MARSCH, E., TU, C.-Y., PEDERSEN, A., RÈME, H. & TROTIGNON, J.-G. 2011 Multi-scale anti-correlation between electron density and magnetic field strength in the solar wind. *Astrophys. J.* **728** (2), 146.

ZANK, G.P. & MATTHAEUS, W.H. 1990 Nearly incompressible hydrodynamics and heat conduction. *Phys. Rev. Lett.* **64** (11), 1243–1246.

ZANK, G.P. & MATTHAEUS, W.H. 1993 Nearly incompressible fluids. II: magnetohydrodynamics, turbulence, and waves. *Phys. Fluids* A **5** (1), 257–273.

ZANK, G.P., NAKANOTANI, M. & WEBB, G.M. 2019 Compressible and incompressible magnetic turbulence observed in the very local interstellar medium by voyager 1. *Astrophys. J.* **887** (2), 116.

ZANK, G.P. & MATTHAEUS, W.H. 1992 Waves and turbulence in the solar wind. *J. Geophys. Res.* **97** (A11), 17189–17194.

ZANK, G.P., MATTHAEUS, W.H. & KLEIN, L.W. 1990 Temperature and density anti-correlations in the solar wind. *Geophys. Res. Lett.* **17**, 1239–1242.